FAKULTA MECHATRONIKY,
INFORMATIKY A MEZIOBOROVÝCH
STUDIÍ TUL

Diplomová práce

Laser-based formation of circuits on sustainable flexible graphene oxide films

Studijní program: N0719A270001 Nanotechnologie
Autor práce: **Bc. Jan Braun**
Vedoucí práce: Dr. Rafael Torres
Ústav nových technologií a aplikované informatiky

Konzultant práce: Ing. Ondřej Havelka
Oddělení environmentální chemie

Liberec 2024

FAKULTA MECHATRONIKY,
INFORMATIKY A MEZIOBOROVÝCH
STUDIÍ TUL

Zadání diplomové práce

Laser-based formation of circuits on sustainable flexible graphene oxide films

Jméno a příjmení:	**Bc. Jan Braun**
Osobní číslo:	M22000063
Studijní program:	N0719A270001 Nanotechnologie
Zadávající katedra:	Katedra chemie
Akademický rok:	2023/2024

Zásady pro vypracování:

1. The primary aim of this diploma thesis is to utilize femtosecond pulsed radiation to reduce graphene oxide (GO) sheets embedded in a flexible film made from a polymeric matrix derived from the natural tree exudate known as ”gum Carrageenan”, known as a highly sustainable polymer. As a study by Senyuk et al. demonstrated, applying femtosecond radiation to GO enables oxygen extraction from its carbonaceous structure, resulting in the material’s reduction. When this reduction occurs within a three-dimensional network, the reduced GO (rGO) exhibits conductivity in contrast to the electrically insulating GO surrounding it. Consequently, this polymeric composite has the potential to serve as a flexible circuit composed of biodegradable materials, promoting sustainability in the field of electronics.
2. Within the implementation of the current research work, we also aim to investigate and optimize the parameters of femtosecond pulsed laser irradiation to efficiently reduce GO to rGO while maintaining the desired electrical conductivity and structural integrity. This objective will focus on understanding the laser’s energy density, pulse duration, repetition rate, and other relevant parameters to achieve the best reduction results.
3. Finally, we will conduct a comprehensive characterization of the developed composite films, including their structural and electrical properties. For this, we will employ techniques such as Raman spectroscopy, X-ray diffraction, scanning electron microscopy (SEM), and electrical conductivity measurements to assess the quality and performance of the rGO and GO-based films for their use as sustainable circuits.

Rozsah grafických prací:	dle potřeby dokumentace
Rozsah pracovní zprávy:	50 stran
Forma zpracování práce:	tištěná/elektronická
Jazyk práce:	angličtina

Seznam odborné literatury:

1. SENYUK, Bohdan, et al. Three-dimensional patterning of solid microstructures through laser reduction of colloidal graphene oxide in liquid-crystalline dispersions. Nature communications, 2015, vol. 6, no 1, p. 7157.
2. KASISCHKE, Maren, et al. Simultaneous nanopatterning and reduction of graphene oxide by femtosecond laser pulses. Applied Surface Science, 2018, vol. 445, p. 197-203.
3. YUAN, Yongjiu, et al. Laser photonic-reduction stamping for graphene-based micro-supercapacitors ultrafast fabrication. Nature communications, 2020, vol. 11, no 1, p. 6185.
4. ZOU, Tingting, et al. High-speed femtosecond laser plasmonic lithography and reduction of graphene oxide for anisotropic photoresponse. Light: Science & Applications, 2020, vol. 9, no 1, p. 69.
5. LI, Qiang, et al. Periodic nanopatterning and reduction of graphene oxide by femtosecond laser to construct high-performance micro-supercapacitors. Carbon, 2021, vol. 172, p. 144-153.
6. LAI, Danning, et al. Comprehensive properties of photodynamic antibacterial film based on κ-Carrageenan and curcumin-β-cyclodextrin complex. Carbohydrate Polymers. Online. April 2022. Vol. 282, p. 119112.
7. PADINJAREVEETIL, Akshay Kumar K.; PADIL, Vinod V. T.; ČERNÍK, Miroslav. Graphene Oxide-Based Nanocomposite and Their Biomedical Applications. Nanoengineering of Biomaterials, 2022, p. 427-456.
8. VENKATESH, Abhilash; PADIL, Vinod VT. Extraction and physicochemical characterization of exudate gums. In the Handbook of Natural Polymers, Volume 1. Elsevier, 2023. p. 577-596.
9. RAMAKRISHNAN, Rohith K., et al. Regenerable and Ultraflexible Sustainable Film Derived from Tree Gum Kondagogu... ACS Sustainable Chemistry & Engineering, 2023, vol. 11, no 19, p. 7344-7356.
10. IZAWA, Hironori, et al. Hierarchical surface wrinkles and bumps generated on chitosan films having double-skin layers... Carbohydrate Polymers. Online. May 2022. Vol. 284, p. 119224.
11. XU, Huan, et al. Graphene oxide-driven design of strong and flexible biopolymer barrier films... ACS Sustainable Chemistry & Engineering, 2016, vol. 4, no 1, p. 334-349.
12. CHRISTIAN, Meganne; MAZZARO, Raffaello; MORANDI, Vittorio. Bioinspired Design of Graphene-Based Materials. Advanced Functional Materials, 2020, vol. 30, no 51, p. 2007458.
13. XIANG, Huacui, et al. Green flexible electronics based on starch. npj Flexible Electronics, 2022, vol. 6, no 1, p. 15.

Vedoucí práce:	Dr. Rafael Torres Ústav nových technologií a aplikované informatiky
Konzultant práce:	Ing. Ondřej Havelka Oddělení environmentální chemie
Datum zadání práce:	11. října 2023
Předpokládaný termín odevzdání:	14. května 2024

L.S.

prof. Ing. Zdeněk Plíva, Ph.D.
děkan

prof. Ing. Josef Šedlbauer, Ph.D.
garant studijního programu

V Liberci dne 13. listopadu 2023

Prohlášení

Prohlašuji, že svou diplomovou práci jsem vypracoval samostatně jako původní dílo s použitím uvedené literatury a na základě konzultací s vedoucím mé diplomové práce a konzultantem.

Jsem si vědom toho, že na mou diplomovou práci se plně vztahuje zákon č. 121/2000 Sb., o právu autorském, zejména § 60 – školní dílo.

Beru na vědomí, že Technická univerzita v Liberci nezasahuje do mých autorských práv užitím mé diplomové práce pro vnitřní potřebu Technické univerzity v Liberci.

Užiji-li diplomovou práci nebo poskytnu-li licenci k jejímu využití, jsem si vědom povinnosti informovat o této skutečnosti Technickou univerzitu v Liberci; v tomto případě má Technická univerzita v Liberci právo ode mne požadovat úhradu nákladů, které vynaložila na vytvoření díla, až do jejich skutečné výše.

Současně čestně prohlašuji, že text elektronické podoby práce vložený do IS/STAG se shoduje s textem tištěné podoby práce.

Beru na vědomí, že má diplomová práce bude zveřejněna Technickou univerzitou v Liberci v souladu s § 47b zákona č. 111/1998 Sb., o vysokých školách a o změně a doplnění dalších zákonů (zákon o vysokých školách), ve znění pozdějších předpisů.

Jsem si vědom následků, které podle zákona o vysokých školách mohou vyplývat z porušení tohoto prohlášení.

13. května 2024 Bc. Jan Braun

Laserem zajištěná tvorba elektrických obvodů na udržitelných a flexibilních filmech z oxidu grafenu

Abstrakt

Tato diplomová práce se zabývá vývojem a následnou redukcí flexibilních a vysoce udržitelných kompozitních materiálů složených z karagenanové matrice a disperze grafen oxidu (GO). Proces redukce je realizován pomocí femtosekundového laserového záření. Jednou z hlavních výhod představené metody, na rozdíl od alternativních redukčních technik, je možnost lokálního vzorování a redukce povrchu GO v jednom jediném kroku bez nutnosti speciálních fyzikálních nebo chemických podmínek. Rozdílem oproti jiným studiím, bylo zanesení GO disperze přímo do polymerní sítě karagenanové matrice a následné ozařování těchto GO vloček přímo uvnitř struktury polymeru. Výsledné filmy vykazovaly rozdílnou morfologii, různé stupně redukce a úrovně vodivosti v závislosti na koncentraci GO vloček. Prostřednictvím komplexní analýzy zahrnující řadu zobrazovacích a analytických technik, které jsou objasněny v experimentální části této práce, se ukazuje, že filmy vyrobené zvoleným přístupem nejsou vhodné pro použití v oblasti flexibilních obvodů. Ačkoli všechny filmy obsahující karagenanovou matrici vykazovaly pozoruhodnou flexibilitu, vodivost byla spíše podprůměrná. I přesto, že se vodivost po ozáření zvyšuje, není ani zdaleka dostačující pro vedení elektrického proudu. Na druhou stranu, tyto výsledky otevírají cestu novým pohledům na celou problematiku a možnosti vylepšení syntézy těchto flexibilních kompozitních filmů, přičemž návrh nové metodologie je diskutován v závěru práce.

Klíčová slova: Flexibílní obvody, karagenan, oxid grafenu, redukovaný oxid grafenu, femtosekundová laserová redukce

Laser-based formation of circuits on sustainable flexible graphene oxide films

Abstract

This diploma thesis focuses on the development and subsequent reduction of highly sustainable and eco-friendly composite materials containing a carrageenan matrix and graphene oxide (GO). The reduction process is carried out utilizing femtosecond laser radiation. One major benefit of this method, in contrast to alternative reduction techniques, is its capability for localized patterning and reduction of the GO surface in a single step, eliminating the necessity for specific physical or chemical conditions. Diverging from prior research, this study introduced GO directly into the polymer network of the carrageenan matrix and then subjected these GO flakes to irradiation within the polymer structure. The resultant films displayed diverse morphology, varying degrees of reduction, and conductivity levels contingent upon the concentration of GO flakes. Through comprehensive analysis, involving an array of imaging and analytical techniques elucidated in the experimental section of this work, it becomes apparent that films produced using the chosen approach are unsuitable for utilization in flexible circuits. Although all films incorporating the carrageenan matrix exhibited noteworthy flexibility, conductivity performance was subpar. Despite an enhancement in conductivity post-irradiation, it remained inadequate for efficient electric current conduction. Nonetheless, these outcomes pave the way for fresh perspectives and enhancements in the synthesis of these flexible composite films, with a new methodology proposition being discussed in the conclusion of the thesis.

Keywords: Flexible circuits, carrageenan, graphene oxide, reduced graphene oxide, femtosecond laser reduction

Acknowledgements

First and foremost, I am grateful to my diploma thesis supervisor, Dr. Rafael Omar Torres Mendieta, for his guidance, insightful suggestions, and unwavering positivity during our collaborative efforts. Secondly, my appreciation goes to Ing. Ondřej Havelka for his consultations and recommended adjustments to the thesis, despite his ongoing foreign internship.

Moreover, my thanks are due to Dr. Daniele Silvestri and Michal Salava for their assistance in the preparation of the composite films, Dr. Pavel Kejzlar and Ing. Michaela Petržílková for providing images obtained through scanning electron microscopy and other related analyses, Dr. Jana Müllerová and Ing. Martin Stuchlík for conducting FTIR measurements and Raman spectrometry, and Dr. Martin Cvek for performing XRD measurements. Additionally, I appreciate the opportunity to engage in research activities as a scientist at the Institute for Nanomaterials, Advanced Technologies, and Innovation (CxI).

Lastly, I would like to express my gratitude to my family and girlfriend for their unwavering support, especially during the challenging moments we have faced together recently.

During the preparation of this study, the author utilized SciSpace for the purpose of revising and modifying the text. Subsequent to employing this tool, the author reviewed and edited the content as needed and takes full responsibility for the content of the diploma thesis.

Contents

List of abbreviations

AG	**A**nhydrous **G**alactose
ATR	**A**ttenuated **T**otal **R**eflectance
BSE	**B**ack**S**cattered **E**lectrons
CNTs	**C**arbon **N**anotubes
CGs	**C**arrageenans
CIFs	**C**rystallographic **I**nformation **F**iles
COD	**C**rystallography **O**pen **D**atabase
CVD	**C**hemical **V**apor **D**eposition
DC	**D**irect **C**urrent
EBSD	**E**lectron **B**ack**S**catter **D**iffraction
EDS	**E**nergy-**D**ispersive X-ray **S**pectroscopy
Fs-LrGO	**F**emtosecond-**L**aser-**r**educed **G**raphene **O**xide
FTIR	**F**ourier **T**ransform **I**nfrared spectroscopy
GO	**G**raphene **O**xide
HSFL	**H**igh-**S**patial-**F**requency **L**IPSS
LIPSS	**L**aser-**I**nduced **P**eriodic **S**urface **S**tructures
LSFL	**L**ow-**S**patial-**F**requency **L**IPSS
MAUD	**M**aterials **A**alysis **U**sing **D**iffraction
NPs	**N**ano**p**articles
RFID	**R**adio **F**requency **I**dentification
rGO	**r**educed **G**raphene **O**xide
PFIB	**P**lasma-**F**ocused **I**on **B**eam
SE	**S**econdary **E**lectrons
SEM	**S**canning **E**lectron **M**icroscopy
SPPs	**S**urface **P**lasmon **P**olaritons
UV-Vis	**U**ltraviolet-**V**isible
XRD	**X**-**R**ay **D**iffraction

List of Figures

List of Tables

1 Introduction

Nowadays, the landscape of electronic devices is experiencing a significant transformation, shifting from rigid, long-lasting, standardized models to wearable, high-performing, and multifunctional components [1]. Among these advances, flexible electronics have emerged as a notable innovation. Soft, stretchable substrates play a crucial role in the fabrication of flexible electronics, with polymer films like polyethylene terephthalate [2], polyimide [3], and various elastomers [4] being commonly utilized for this purpose. However, a major drawback associated with these substrates is their lack of degradability, which raises concerns about the accumulation of electronic waste in the future. Addressing this issue is imperative for sustainable technological progress [5].

One potential avenue for resolving this challenge lies in utilizing substrates derived from natural materials such as polysaccharides, lipids, and proteins. These materials offer the advantages of abundant availability, non-toxic properties, and rapid decomposition under specific environmental conditions [6]. Carrageenans, a type of natural polysaccharide extracted from red seaweed, stand out as a particularly promising option. In addition to the favorable attributes mentioned earlier, carrageenans demonstrate exceptional gelling and film-forming capabilities [7]. Films derived from carrageenan are inherently biodegradable, with the ability to decompose almost entirely within a week when exposed to soil, presenting a viable pathway for the development of eco-friendly films [8].

Nevertheless, the presence of a flexible substrate alone does not suffice to create a flexible circuit. It is essential to establish paths of conductive material on the substrate's surface, with various metals being the preferred choice due to their low resistivity and high conductivity [9]. For example, copper is renowned for its exceptional conductivity, characterized by a resistivity value on the order of $1.72 \cdot 10^{-8}$ $\Omega \cdot m$. However, the finite nature of metal resources raises concerns about their long-term availability, prompting research into alternative conductive components like carbon allotropes, conductive polymers, and ionic liquids as potential substitutes for metals [10]. Graphene, a member of the 2D materials family, possesses unparalleled properties that make it highly appealing for diverse applications. In the realm of flexible circuits, its remarkable electrical conductivity and flexibility are particularly advantageous [11]. Nonetheless, the challenges associated with large-scale isolation of graphene contribute to its relatively high cost in manufacturing processes [12].

One of the methods for producing a graphene-like material on an industrial scale involves reducing GO to form rGO. While the conductivity of rGO may not match that of pristine graphene, it is deemed adequate for the development of circuits [13]. Moreover, the easy dispersibility of GO in water enables solution processing, making it compatible with various flexible electronics manufacturing techniques like inkjet printing and dip-coating [14]. The presence of oxygen-containing groups and defects in the carbon structure of GO renders it a compelling material for diverse applications, particularly due to the dielectric properties conferred by the oxygen-containing groups [15]. Laser reduction methods, notably, are favored for reducing GO as they allow high-speed local patterning of GO without necessitating specific physical or chemical conditions. This approach streamlines the reduction of the GO surface while simultaneously tailoring it to the desired pattern, proving to be an efficient strategy for producing electrical circuits [16].

This study delves into the fabrication and laser reduction of carrageenan-based composite films incorporating dispersed GO flakes, with variations in structural and electrical characteristics achieved through different GO concentrations. The GO utilized in this research will be obtained through electrochemical exfoliation, a highly promising environmentally friendly technique known for its high efficiency and cost-effectiveness [17]. For the manufacturing of flexible films, a straightforward experiment was selected, specifically the direct incorporation of GO into the polymer matrix. This choice aims to guarantee the films' exceptional sustainability and the feasibility of mass production. Following this, the films' surface underwent irradiation with femtosecond laser radiation, with the expectation of creating conductive pathways enveloped by an electrically insulating network of the polymer alongside pristine GO. Consequently, this polymer composite holds potential as a sustainable flexible circuit composed of biodegradable materials, thereby advancing sustainability in the realm of electronics.

The theoretical segment aims to acquaint the reader with flexible circuits, carrageenans, graphene, and GO, offering insights into their structures, properties, applications, and production methodologies. Notably, the section scrutinizes rGO, focusing on various GO reduction techniques, with a detailed exploration of reduction via femtosecond laser radiation and its potential mechanism. The experimental phase of the study is primarily geared towards fabricating the previously outlined highly sustainable flexible films based on carrageenan and elucidating their properties through a diverse array of characterization techniques.

2 Flexible circuits

The notion of flexible electronics has been around for many years. Essentially, anything that is thin or elongated can be rendered flexible. Advancements in conductive polymers, organic semiconductors, and amorphous silicon have significantly enhanced flexibility and processability, making these materials the foundation for electronic devices in scenarios necessitating bending, rolling, folding, stretching, and other characteristics that traditional electronics cannot provide [18]. The interpretation of flexibility varies based on the specific application. It ranges from bending and rolling for the easier manipulation of large-area photovoltaics to conforming to irregular shapes, folding, twisting, stretching, and deforming for electronic skin devices, all while upholding device performance and dependability [19]. Flexible circuits are a crucial element of flexible electronics, typically built on flexible substrates. The interest in this field has expanded to encompass not just flexibility but also attributes like stretchability - the capacity of a circuit to endure substantial stresses without failing, and healability, which can be accomplished by using elastomeric substrates with robust molecular interactions [20]. Similarly, biocompatibility and biodegradability have been made possible through polymers that do not cause harm to the body and can be disintegrated into smaller components post-use [19].

The advancement of flexible circuits frequently involves the combination of a variety of materials, including organic semiconductors, inorganic nanomaterials such as nanowires and nanotubes, and thin oxide films to achieve specific characteristics [21]. The challenge, however, remains in developing a rapid and cost-efficient approach to creating highly conductive flexible circuits, a key hurdle in bridging the gap between laboratory-scale experimentation and industrial implementation. Various innovative techniques like nanoimprinting, screen printing, dip-pen lithography, microcontact printing, inkjet printing, and LightScribe have been utilized for fabricating micro- or nano-flexible circuits [22]. A clear example of this is the case of a method that involves using silver nanowires as foundational elements on polydimethylsiloxane films to construct flexible circuits [23]. Inkjet printing has also been applied to produce extensive flexible circuits with exceptional electrical conductivity and mechanical flexibility [24]. Laser processing, in addition, has been employed to generate circuit patterns on flexible substrates, enabling the development of multi-layered circuits for flexible electronics [16, 25]. Creating flexible circuits, therefore, encompasses a blend of inventive materials, printing technologies, and patterning techniques to achieve high-performance, malleable, and stretchable electronic components.

Because of these characteristics, flexible circuit technology has rapidly found its way into various applications (Fig. 2.1) and has become a key component in numerous products, progressing towards developing modern, flexible electronics that often possess stretchability characteristics [20]. These flexible electronics encompass lighting and display technologies utilized in consumer electronics, architecture, textiles, and wearable devices embedded with sensors to monitor health and behavior [26]. Moreover, they include implantable electronics for enhanced medical imaging and diagnostics and contribute to enhancing the capabilities of robots and unmanned aircraft through lightweight and adaptable energy-harvesting devices and sensors [27].

In the present era, there is a rising focus on ecology and environmental issues, with a growing concern for the future. Yet, the annual production of electronic devices keeps rising, often incorporating polymers as a base material (e.g. polyethylene terephthalate, polyimide), which are usually resistant to degradation [28]. Thus, the widespread use of these materials raises concerns about the rapid accumulation of electronic waste. To give an idea of this problem's magnitude, the estimation for the worldwide production of electronic waste escalated to 53.6 million tons as of the year 2020, translating to an average of 7.3 kg per individual. This is a figure that could surge to a staggering 74.7 million tons by 2030. Surprisingly, in the year 2019, only 17.4 % of the electronic waste generated was subjected to the recycling process, primarily due to the complexities involved in the recycling procedures and the presence of suboptimal policies governing the recycling industry [6]. Environmentally friendly functional electronic devices with strong degradability could offer a solution to this issue. Polysaccharides like carrageenans, being among the most abundant natural polymers, have demonstrated significant potential for the creation of eco-friendly functional electronics due to their cost-effectiveness, ease of processing, and ability to biodegrade, e.g., in soil [8].

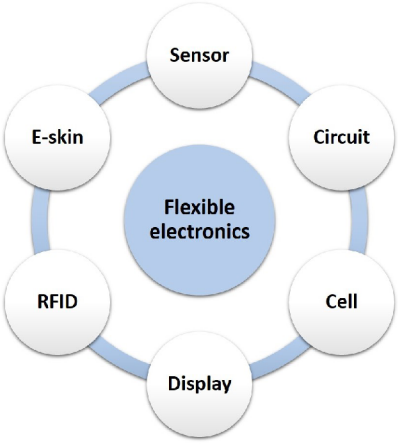

Figure 2.1: An illustrative depiction showcasing the primary use of flexible electronics and its influence on society

3 Carrageenan

With the increasing awareness of environmental conservation, there is a growing interest in bio-based polymers due to their abundant availability, non-toxic nature, and ability to degrade rapidly under specific temperature and humidity conditions. Consequently, various biomaterials, including polysaccharides, lipids, and proteins, are continually under scrutiny [6]. Among these, carrageenans (CGs), rich in hydroxyl groups, are particularly promising, not only for their aforementioned attributes but also for their remarkable gelling and film-forming capabilities [7]. Moreover, films derived from CG can almost completely degrade within a week when exposed to soil, offering the potential for producing environmentally friendly and readily degradable films [8].

CGs are polysaccharides extracted from specific types of red seaweed such as *Eucheuma cottonii*, *Mastocarpus stellatus*, and *Hypnea musciformis* [7]. Typically, commercial seaweeds contain 30-60 % CG by dry weight, but this can reach 70-80 %. CG is found in both the cell wall and the intercellular matrix of plant tissue, with minimal cellulosic material forming the core of microfibrils positioned around the outer cell wall for reinforcement [29]. These seaweed species consist of copolymers of 3,6-anhydrous-galactose (3,6-AG) and D-galactose connected by $\alpha - 1,3$ and $\beta - 1,4$-glycosidic bonds. Traditionally, CGs are categorized into six main types - Iota (ι)-, Kappa (κ)-, Lambda (λ)-, Mu (μ)-, Nu (ν)- and Theta (θ)- CG, based on the number and positions of sulfate groups, a classification crucial for both chemical identification and industrial production due to the different sources of CG subtypes [30].

The three most significant commercial CGs are ι-, κ-, and λ-CG. The dimers of κ-, ι- and λ-CG contain one, two, and three sulfate ester groups, respectively, resulting in calculated sulfate contents of 20%, 33%, and 41% (w/w) respectively. As each natural CG is a complex polysaccharide based on galactose, with varying quantities of sulfate esters at different positions and distributions, the term disaccharide repeating unit is used to describe the idealized structure [29]. For instance, the configuration of κ-CG, utilized in the context of this study, is depicted in Figure 3.1.

CGs are insoluble in organic solvents, oils, and fats but soluble in water. Solubility in water is primarily influenced by the levels of sulfate groups (highly hydrophilic) and the accompanying cations [8]. The primary ionizable cations present in CGs

include sodium, potassium, calcium, and magnesium. Therefore, the ratio of sulfate fractions and the balance of cations in the water solution play a key role in determining the viscosity of solutions or the strength of gels formed by CGs [31].

Various techniques can be utilized for CG extraction, such as alkaline solvents, ultrasonic-assisted, and microwave-assisted methods. While alkaline solvents are the most commonly employed, they are complex and time-consuming [32], whereas ultrasonic-assisted and microwave-assisted methods offer several advantages. These methods have shorter extraction times, lower energy consumption, and higher yields, making them increasingly popular. For instance, ultrasonic extraction can yield 50–55 % of CGs in just 15 minutes with an ultrasound power of 150 W [33]. Moreover, microwave-assisted extraction is useful for samples with high moisture content, as it can quickly heat both the samples and the solvent. However, proper parameter adjustments are crucial, as they significantly impact the yield of CGs [34]. It's also important to note that these extraction methods can affect the structure, bioactivity, and composition of CGs. Therefore, the future direction of CGs extraction methods is likely to involve a combination of various extraction technologies.

Regarding their applications, CGs have a broad spectrum of potential utilization in various fields owing to their diverse characteristics and uses. Within the food industry, CGs are extensively employed for their thickening, gelling, and stabilizing properties. They serve as binders and stabilizers in meat-processing applications, contributing to producing items like patties, sausages, and low-fat hamburgers [35]. Additionally, CGs play a significant role in developing packaging materials with unique properties for food-related purposes [36]. In cosmetic products, CG is used in everyday products such as soap, toothpaste, and sunscreen cream, mainly serving as moisturizing and stabilizing agents [37]. Furthermore, CG oligosaccharides, the byproducts of CG degradation, show diverse biological effects on human health, such as antioxidant, antitumor, immunomodulatory, anti-inflammatory, and antiviral activities [7]. Lastly, due to their exceptional gelling and film-forming capabilities, CGs could theoretically be used for the production of sustainable, flexible, and biodegradable films. These films could serve as a basis for eco-friendly flexible circuits, where metals could potentially be replaced by more sustainable and available compounds such as graphene, GO, and its reduced form [6, 8, 38].

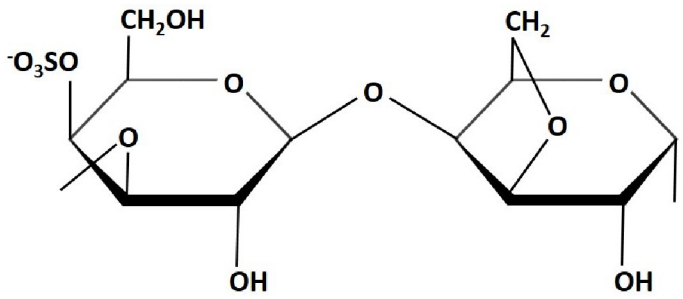

Figure 3.1: Chemical structure of κ-CG

4 Graphene and its derivatives

4.1 Graphene

In nature, the materials chosen for a specific purpose are primarily determined by their availabilities at the precise moment they are required. To date, scientists specializing in materials have a wide range of materials at their disposal, each with distinct properties, enabling them to craft composites and devices inspired by biological systems and which can even surpass their natural counterparts in terms of performance [38]. Among these materials, graphene stands out prominently. This two-dimensional wonder, part of the illustrious 2D materials family, was unveiled to the world's scientific community as an easily accessible material in 2004 by Andre Geim and Konstantin Novoselov, distinguished researchers from the University of Manchester, United Kingdom, who were honored with the Nobel Prize in Physics in 2010 for their breakthrough. Through a methodical process involving adhesive tape and carefully peeling layers from highly oriented pyrolytic graphite, they isolated a single atomic layer, now renowned as graphene [39]. This mechanical exfoliation method is just one facet of graphene's intricate synthesis, explored further in subsequent sections. Notably, the roots of graphene research trace back to the mid-20th century, with Canadian physicist P. Wallace's theoretical musings on 2D carbon nanostructures [40]. Building on this foundation, Boehm and Hofmann made strides in the 1960s, endeavoring to create ultrathin layers of reduced graphite oxide. It was not until 1986 that the term "graphene" found its place in scientific discourse, thanks to Boehm and colleagues [41].

Graphene, a marvel of carbon allotropy, manifests as a single layer of tightly knit carbon atoms, arranged in a hexagonal lattice akin to a honeycomb (Fig. 4.1). This lattice serves as the cornerstone for various carbon configurations; its layers may be fashioned into 0D fullerene, rolled into 1D nanotubes, or stacked to form 3D graphite [42]. According to the ISO/TS 21356-1:2021, graphene can only consist of a maximum of 10 layers; any more layers are classified as graphite instead of graphene. The carbon atoms present in the structure exhibit sp^2 hybridization, which is a phenomenon that occurs when the electron orbitals of the carbon atom are rearranged to form three new hybrid orbitals that are in a combination of s and p orbitals [43]. This hybridization facilitates the formation of three sigma bonds, resulting in a trigonal planar geometry, each bond measuring approximately 0.142 nm. Simultaneously, the fourth electron in the p_z orbital forms a π bond oriented

out-of-plane, as it overlaps with neighboring orbitals. Collectively, these π bonds contribute to the formation of π-bands and π^*-band, underpinning graphene's distinctive electrical properties [44, 45]. Furthermore, these properties are intricately tied to the surface morphology of both the graphene and its substrate [46].

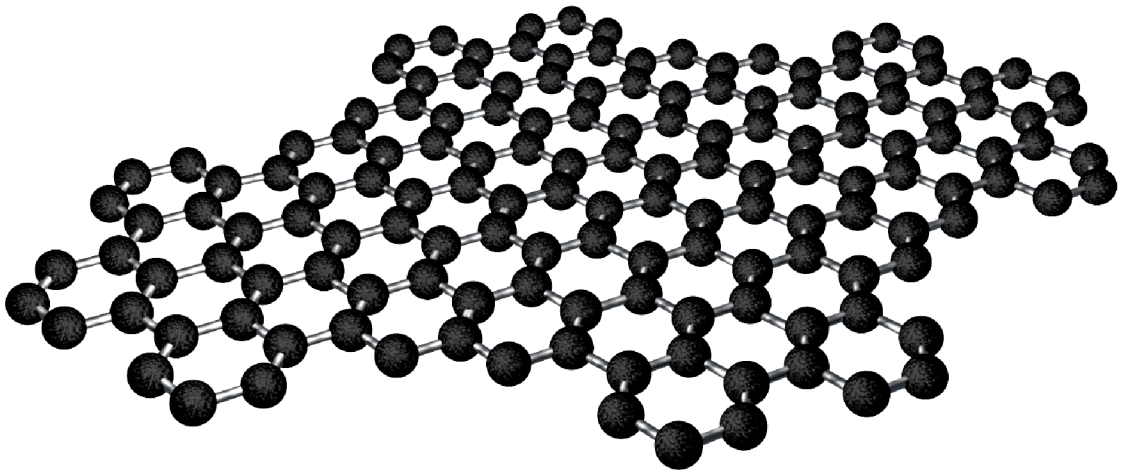

Figure 4.1: Ideal graphene structure

Graphene boasts an extraordinary array of properties poised for application in crafting materials with diverse and remarkable characteristics [11]. While graphite is typically viewed as an inorganic compound due to its relatively inert nature, graphene exists in a realm of ambiguity, embodying both organic and inorganic properties within its structure. This duality becomes particularly pronounced when graphene undergoes oxidation, transforming into GO, which features functional groups mirroring those found in organic compounds like proteins and biopolymers [38]. In terms of its intrinsic properties, graphene showcases an exceptionally vast theoretical specific area, measuring approximately 2630 $m^2 \cdot g^{-1}$, marking a remarkable trait of this material. Moreover, its intrinsic mobility is unparalleled, boasting a theoretical value of 200,000 $cm^2 \cdot V^{-1} \cdot s^{-1}$ [47]. Additionally, it exhibits an extraordinary Young's modulus, which surpasses any other material with a value of approximately 1 TPa. Furthermore, graphene showcases an exceptional thermal conductivity that is significantly high, measuring around 5000 $W \cdot m^{-1} \cdot K^{-1}$ [11]. Despite its single-atom thickness, graphene possesses remarkable light-absorption capabilities, absorbing a significant portion ($\pi\alpha \approx 2.3$ %) of incident white light, where α index belongs to the so-called fine structure constant, which is described by Eq. 4.1. The number of graphene layers can be deduced from its absorbance value, as it grows linearly with the number of layers [48]. Moreover, its exceptional elasticity renders it highly adaptable and flexible [11].

$$\alpha = \frac{e^2}{\hbar c}, \tag{4.1}$$

where e is the elementary charge, $\hbar$ is the reduced Planck constant, c is the speed of light in vacuum.

Given its myriad structural advantages, graphene often earns the title of a revolutionary material [49]. It is hardly surprising, then, that graphene boasts an extensive array of potential applications, only a handful of which are highlighted here. First and foremost, in the realm of electronics, graphene finds its place in high-frequency transistors [50], memory devices [51], flexible circuits [52], and solar cells [53]. Its versatility extends to various sensor types, leveraging not just its conductivity but also the fact that each carbon atom serves as a surface atom [54]. Biomedical research also embraces graphene's potential, employing it in targeted therapy, drug delivery systems, and tissue scaffolding to promote regeneration [55]. Furthermore, due to its mechanical prowess and lightweight nature, graphene integrates seamlessly into various composite materials and numerous other fields [56]. However, it is essential to note that while graphene-based products show immense promise, most are still confined to laboratory settings, with only a handful making it to market [57]. The primary hurdle lies in the cost and quality of graphene production, which often hinders its practical application. Labs worldwide are diligently addressing this challenge, striving to develop a production process that is rapid, scalable, environmentally sustainable, and cost-effective, thus ushering in an era of unparalleled graphene utilization [12].

4.1.1 Graphene synthesis

Graphene synthesis primarily revolves around two approaches: the top-down and bottom-up methods. In the top-down approach, graphene is derived by isolating and delaminating layers from graphite, whereas the bottom-up method involves chemical reactions to construct graphene from atomic-sized precursors [43]. Various techniques are employed for graphene preparation, including different forms of exfoliation such as mechanical [58], liquid phase [59]), chemical vapor deposition (CVD) [60], thermal decomposition of silicon carbide [61], un-zipping carbon nanotubes (CNTs) [62], and GO reduction [63]. Among these methods, mechanical exfoliation stands out for yielding high-quality graphene from natural multilayered structures or growth substrates. This conventional technique involves interfacial peeling and intralayer tearing, which can be tailored based on material characteristics, geometric structure, and exfoliation kinetics. Despite producing superior graphene, this process is time-intensive and offers low yields, rendering it impractical for industrial-scale production and primarily confined to laboratory research [64].

In CVD, on the other hand, gas species introduced into the reactor traverse a high-temperature zone. At the metal substrate interface, hydrocarbon precursors undergo

decomposition, yielding carbon radicals that self-assemble into graphene layers. The choice of metal substrate, in addition, significantly impacts graphene quality, as it catalyzes the reaction. Transition metals like Pt, Co, Pd, Ni, and Cu are commonly utilized as catalysts [65]. Thus, while CVD holds promise for large-scale graphene production, the subsequent transfer of graphene to an electrically non-conductive substrate presents a significant challenge, particularly for industrial applications. In contrast, thermal silicon carbide decomposition obviates the need for graphene transfer in electronic device synthesis. Brief heating prompts Si atoms to desorb, owing to their higher vapor pressure compared to carbon, leaving behind rearranged carbon atoms forming graphitic layers [61].

Lastly, GO reduction produces rGO, a material akin to graphene. The inclusion of GO and rGO in graphene synthesis expands possibilities for chemical modifications, enhancing applications and easing production of this otherwise inert substance on an industrial scale [16, 66]. Further discussion on this method will be elaborated in the subsection "GO synthesis".

4.2 Graphene Oxide

GO is a remarkable carbon-based material distinguished by its two-dimensional structure. Derived from graphene, GO comprises a single layer enriched with oxygen functional groups, including hydroxyl, carboxyl, and epoxy oxygen groups, distributed across its basal plane and edges. This unique composition results in a blend of sp^2 and sp^3 hybridized carbon atoms. Analogous to graphene, a single-layer structure is termed GO, whereas a structure with eleven or more layers is denoted as graphite oxide [67].

Various models of GO have been proposed through diverse analyses and theoretical simulations. Among these, the L-K model, devised by Lerf and Klinowski in 1998, has gained widespread acceptance, particularly for moderately oxidized GO [68]. The L-K model (Fig. 4.2) delineates two distinct regions within GO: regions characterized by six-membered aliphatic rings and those featuring nonoxidized benzene aromatic rings. The extent of material oxidation determines the size of these regions. According to this model, hydroxy and epoxy groups attach to the layer of aliphatic and aromatic six-membered carbon rings, while carbonyl and carboxyl groups are predominantly situated around the edges [69]. However, actual GO may exhibit imperfections such as topological defects, adatoms, vacancies, and adsorbed impurities [70].

The properties of GO heavily rely on the synthesis method employed, which influences the type and quantity of oxygen-containing groups present in the material [71]. In contrast to its hydrophobic precursor, graphene, GO displays a hydrophilic nature, enabling it to disperse readily in various solvents, particularly water. Additionally, the oxygen-containing functional groups serve as reactive sites for chemical

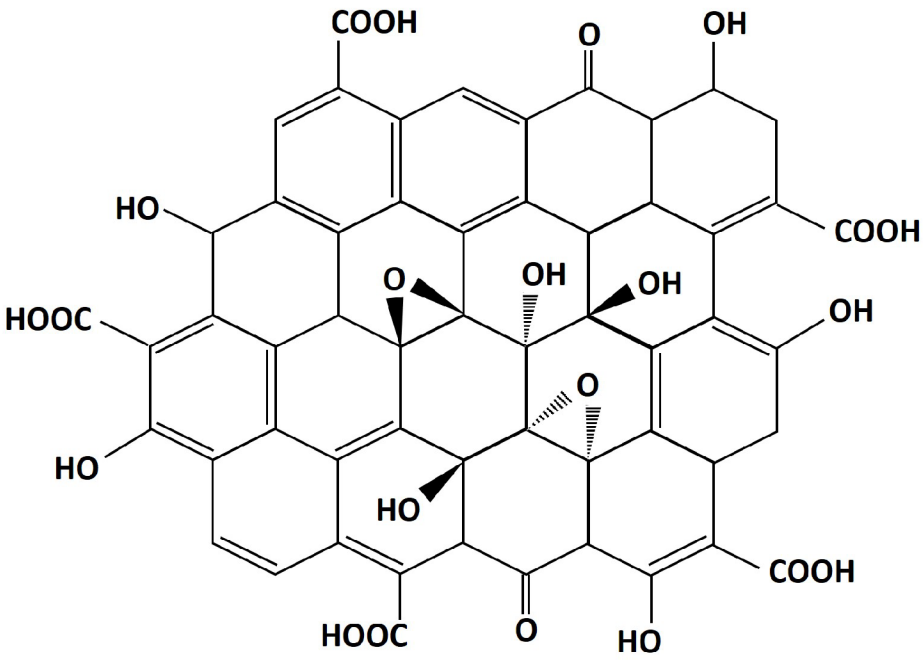

Figure 4.2: Chemical structure of GO based on L-K model

modification or functionalization of GO, thereby facilitating the development of GO-based materials [14]. Moreover, GO serves as a versatile precursor for synthesizing graphene derivatives such as fluorographene, bromographene, and graphane, among others [68]. While these oxygen-containing groups can mitigate certain drawbacks of graphene, they can also render GO electrically insulating [15].

4.2.1 GO synthesis

The process of synthesizing GO begins with the oxidation of graphite powder to create graphite oxide, followed by exfoliating its particles using ultrasound to produce flakes of GO. Various methods are employed in the synthesis of graphite oxide, including the classic Hummers method, Brodie method, Staudenmeier method, and Tour method [71]. Additionally, GO can also be formed during the electrochemical exfoliation process when graphite electrodes are utilized in the presence of sulfuric acid or other acidic electrolytes [72]. These methods offer a range of choices for researchers seeking to synthesize graphite oxide for different applications in the field of materials science.

The Hummers and Offeman method, published in 1958, is widely recognized as a classic and commonly used approach. This method, known for its relative rapidity, offers a safer alternative to chlorate-based methods such as the Brodie and Staudenmeier methods [73]. Its enhanced safety stems from the prevention of explosive ClO_2 formation during the reaction. The Hummers method involves the use of an excess of potassium permanganate, sulfuric acid, and a small quantity

of sodium nitrate on graphite. Upon completion of the reaction, any excess potassium permanganate is neutralized using a diluted H_2O_2 solution, resulting in the formation of non-toxic byproducts that can be easily eliminated. Despite its ability to yield a considerable amount of colloidal suspension and powder product, this method falls short of environmental standards due to the release of NO_x during the reaction. Additionally, the resulting GO often contains traces of sulfur (up to 6 %) and nitrogen, likely due to covalently bound sulfates and nitrates or adsorbed sulfuric and nitric acids. Consequently, various research groups have made strides in refining the preparation method [74].

A notable improvement came in 2010 with the development of a refined technique to GO with a heightened degree of oxidation by modifying the Hummers method. Instead of sodium nitrate, phosphoric acid (H_3PO_4) was employed to facilitate oxidative chemical exfoliation of graphite, resulting in a higher yield of GO [75]. Phosphoric acid serves multiple functions as a dispersing and etching agent, as well as a stabilizer of the oxidation process, ensuring the safety of GO synthesis. Compared to other preparation methods, GO produced using the Tour method exhibits a greater degree of oxidation and a more regular structure with fewer defects in the basal plane [76]. However, a drawback is that the oxidation time for graphite to be converted into GO using Tour's method is more time-consuming than the Hummers method, rendering it economically impractical for large-scale GO production [77].

Unlike these synthetic practices, electrochemical exfoliation emerges as a promising avenue for large-scale graphene or GO production, offering notable benefits such as high productivity, cost-effectiveness, and environmentally friendly processes [78]. This method achieves graphite exfoliation by continually intercalating electrolyte ions or charged particles into the graphitic layers, facilitated by either cathodic or anodic potential. Cation intercalation, for instance, circumvents the need for oxidizing conditions, thereby averting the introduction of oxygen-containing groups into the final graphene products. However, this typically yields multilayer graphene, necessitating laborious isolation. Conversely, anion intercalation is a swifter process, often completed in less than an hour. Nevertheless, employing positive potentials in anion intercalation results in the decoration of graphene with functional oxygen groups, especially evident when sulfuric acid or other acidic electrolytes are employed [79]

4.3 Reduced Graphene Oxide

GO can recover its graphene-like properties through additional reductive exfoliation processes, transforming into a material closely resembling graphene, known as rGO [80]. However, rGO retains some introduced groups from the oxidation process within the GO layer, particularly those resistant groups located at the edges, leading to distinct properties, notably reduced conductivity compared to graphene [13]. Despite this, the process provides a cost-effective and scalable means

for producing graphene-based materials in large quantities, making rGO a practical compromise between graphene and GO [81]. Moreover, the characteristics of rGO can be finely tuned by controlling the extent of GO reduction, offering manipulation of crucial properties through the regulation of the reduction procedure [13].

Various techniques, including chemical, thermal, and light-assisted treatment and reduction mediated by biological microorganisms, have been employed for GO reduction, each with its own advantages and drawbacks [80]. Chemical reduction is a commonly used method for reducing GO dispersions and large-scale production of graphene powders, either at room temperature or with mild heating. While effective, efficient reducing agents like hydrazine hydrate and sodium borohydride often pose hazards due to their corrosive or explosive nature. Additionally, using surfactants during GO processing requires thorough purification, limiting rGO applications in biological systems [82]. Efforts to find non-toxic alternatives to traditional reducing agents have resulted in substitutes with lower reduction efficiency, which may aggregate due to strong $-$ stacking and Van der Waals interactions between rGO sheets [83].

Thermal reduction involving heating GO to temperatures exceeding 150 °C facilitates converting oxygen-containing groups into volatile compounds. However, to produce highly conductive rGO films, annealing often requires temperatures surpassing 1000 °C, primarily generating CO_2 alongside other substances like CO, H_2O, and various organic molecules [84]. Although less harmful than chemical methods, thermal annealing results in imperfections in rGO films due to elevated defect concentrations caused by the partial removal of carbon alongside functional groups [85].

On the biological front, some microorganisms can metabolize and transfer electrons, inspiring research into rGO synthesis through incubation with microorganisms. For instance, species like *Shewanella* can reduce GO through respiration under anaerobic or aerobic conditions, transferring electrons to GO during bacterial respiration [86].

Light-assisted techniques, such as laser methods, offer advantages over other methods. These techniques allow precise control of the carbon and oxygen atom ratio in GO without impurities and high-speed local patterning of GO without specific physical or chemical conditions. This chemical-free approach enables the creation of conductive patterns with a resolution of up to 1 μm, without the need for clean space and masking required in more costly lithographic methods [87]. Additionally, the laser reduction method permits adjustment of the reduction degree by modifying laser parameters, such as wavelength, mode, pulse duration, power density, and environment, offering versatility compared to many existing methods [13]. This stands in contrast to methods like lithography, which typically involve patterning graphene either before or after production [16].

4.3.1 Mechanism of GO reduction by laser

In recent years, laser reduction of GO has gained significant traction as a straightforward, effective, and cost-efficient technique for material modification [88]. By leveraging the combination of graphene lattice and pulsed laser irradiation under diverse environmental conditions, this method offers avenues for functionalization, reduction, ablation, and the creation of 2D and 3D micropatterns, rendering laser processing highly appealing for the fabrication of graphene-based devices [66]. Figure 4.3 illustrates the intricate interplay between the laser and GO during this process. In this study, we delve into the reduction of GO using femtosecond laser radiation, with a specific focus on elucidating the unique mechanisms associated with this particular pulse duration.

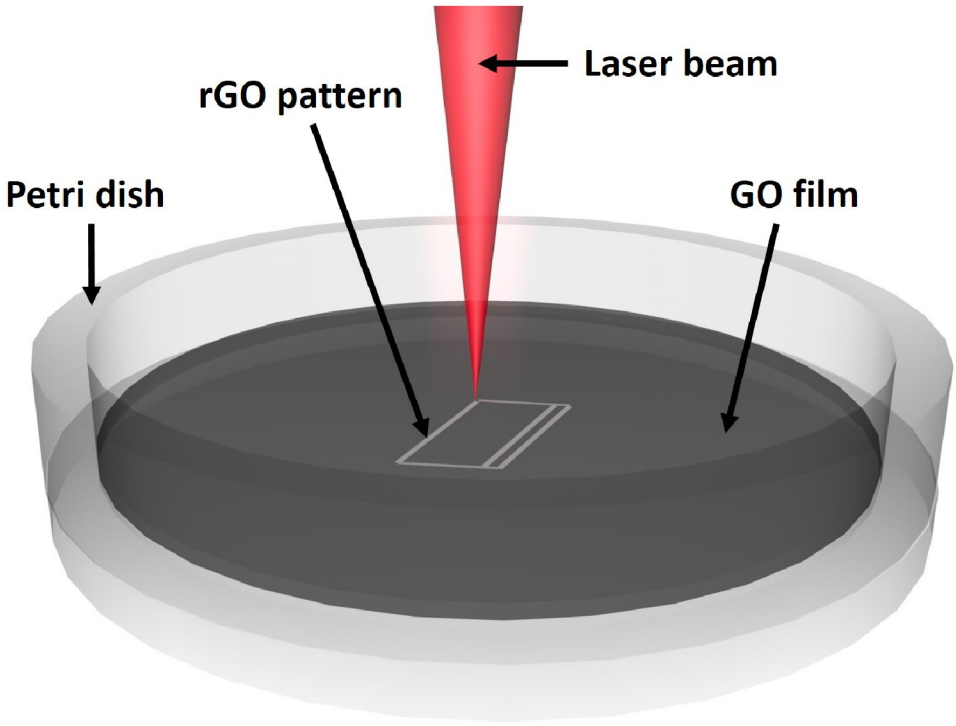

Figure 4.3: The general scheme of the laser reduction of GO in patterned lines

The evolution of graphite structure and changes in chemical content in GO give rise to a unique process of reduction and nanopatterning when employing femtosecond laser pulses, setting it apart from similar processes in other metals, semiconductors, and non-conductors [89]. Laser reduction mechanisms typically fall into two primary categories: photochemical (non-thermal effect) and photothermal reduction (thermal effect). Initially, when femtosecond laser radiation interacts with materials, photochemical reduction initiates a non-thermal, rapid excitation of electrons from bonding to antibonding states. This prompts a significant weakening of the C–O electron bond near the top of the valence band, leading to the immediate elimination of oxygen [63]. Consequently, some weakly bound carbon atoms are

also removed, resulting in an increase in defect density. Femtosecond laser irradiation generates a multitude of excited photons that produce freely moving electrons and holes, facilitating the reduction of GO to rGO [90]. As the process progresses, photothermal reduction gradually takes place, with the cumulative effect of pulsed laser generating heat, inducing the pyrolysis of GO. This leads to the decomposition of oxygen-containing functional groups such as hydroxyl (−OH), carboxyl (−COOH), and oxygen bridges (C−O−C) into CO, CO_2, and H_2O, which are then eliminated [63]. During this phase, the carbon lattice undergoes thermal relaxation, forming conjugated hexagonal sp^2 structures [25].

The fundamental process of periodic nanopatterning and femtosecond laser reduction of GO primarily involves excited surface plasmon polaritons (SPPs) and the photochemical elimination of oxygen-containing groups. Initially, during femtosecond laser-induced periodic nanopatterning, the photochemical impact plays a crucial role in eliminating certain carbonyl and hydroxyl groups situated at the edges of the GO nanosheet due to rapid excitation from the laser pulses [89]. Photochemical reduction of GO occurs when the binding energy of femtosecond-laser-reduced GO (Fs-LrGO) reaches around 9 $mJ{\cdot}cm^{-2}$. Simultaneously, the 2.7 to 3.1 eV energy gap for sp^3 hybridized carbon in GO displays a nonlinear optical response under femtosecond laser irradiation [91]. The two-photon absorption of the sp^3 domains of GO becomes more prominent, transitioning the optical and electrical characteristics of Fs-LrGO from insulating to conducting by a significant increase in excited free electrons. Through the interaction of ultrafast light waves with surface charge oscillation, SPPs on the surface of Fs-LrGO are activated. SPPs are essentially partially longitudinal electromagnetic waves, with their frequency and amplitude dependent on the coupling between the incident laser and excited surface electrons [92]. Moreover, the absorbed laser energy by Fs-LrGO can combine with the SPP to generate an SPP standing wave around specific nanoholes and nanogrooves on the rough surface. Once the accumulated energy from the SPP standing wave surpasses the ablation threshold (20 $mJ{\cdot}cm^{-2}$) required for nanopattern formation, the initial high-spatial-frequency LIPSS (HSFL) is produced. Subsequently, the interaction between HSFL and the incident laser can alter the distribution of SPPs. Low-spatial-frequency LIPSS (LSFL) is created by the interference of light waves and HSFL on the surface. With the increase in incident fluence, the local field enhancement around the laser-induced periodic surface structures (LIPSS) can selectively absorb more laser energy, displaying a resonance enhancement absorption effect. Consequently, the depth of the laser-induced periodic nanopattern escalates, forming 3D cross-linked LIPSS and flake-groove structures due to the local field enhancement effect [89]. Additionally, the sp^3-hybridized carbon atoms are converted to sp^2 hybridization, enhancing the conductivity of Fs-LrGO [25].

The reduction of Fs-LrGO is influenced by various parameters, with the most significant being laser fluence. Adjusting the laser fluence can change the degree of reduction and properties such as structure and conductivity [93]. When the laser fluence is approximately 9 $mJ{\cdot}cm^{-2}$, there is no apparent change in the surface mor-

phology of the irradiated GO, suggesting that the laser energy is below the threshold for Fs-LrGO nanopatterning. As the fluence increases, some LIPSS microwells appear on the irradiated Fs-LrGO surface compared to the original GO surface. At around a fluence of 20 $mJ{\cdot}cm^{-2}$, the area of periodic wavy structures expands, resulting in the reorganization of the graphene structure and a reduction in the degree of Fs-LrGO defects. This fluence level can be seen as a threshold for GO reduction via femtosecond laser [89]. The subwavelength ripples known as HSFL have a periodicity of approximately 100 nm and 120 nm and are perpendicular to the laser beam's polarization [16]. Increasing the fluence to 30 $mJ{\cdot}cm^{-2}$ leads to the emergence of reticulated periodic microstructures on the irradiated surface, including a long-wavelength wavy structure called LSFL, which has a periodicity similar to the laser beam and HSFL wavelengths [89]. The orientation of the LSFL aligns parallel to the laser beam's polarization direction [16]. Further fluence increase transforms cross-linked periodic structures into nanopatterned micro-flakes at 40 $mJ{\cdot}cm^{-2}$. As the fluence reaches 60 $mJ{\cdot}cm^{-2}$, an abundance of laser energy leads to microgroove patterns on the Fs-LrGO surface. Furthermore, substantial laser energy can effectively eliminate GO through irradiation. Hence, it is evident that changes in the incident laser fluence directly impact the morphological evolution in Fs-LrGO [89].

Concerning the electrical conductivity characteristics of the original GO and Fs-LrGO based on various laser fluences, it is commonly observed that the pristine rGO sheet exhibits conductivity levels ranging between 10^4 to 10^1 $S{\cdot}m^{-1}$, attributed to variations in measurement techniques and materials processing [89, 94]. Notably, the conductivity of the Fs-LrGO film shows a progressive rise with increasing laser fluence, primarily attributed to the decrease in oxygen-containing groups, a phenomenon that becomes more pronounced with higher incident fluence [95].

Another critical aspect to consider is the repetition frequency. The ablation threshold is noted to decrease with more intense fluences as the pulse repetition rate transitions from kHz to MHz, a trend likely stemming from cumulative effects resulting from successive pulses [90].

Lastly, in terms of pulse duration, femtosecond laser pulses do not induce substantial heating in the substrate, indicating the feasibility of conducting Fs-LrGO production on thermally sensitive polymers and surfaces [25].

5 Methodology

5.1 GO synthesis

The GO utilized in this study was synthesized via the electrochemical exfoliation technique, a widely adopted method for producing graphene. In this process, a conventional two-electrode system was employed, consisting of two graphite plates serving as the anode and cathode. The electrolyte solution comprised 40 mL of an aqueous solution with a concentration of 0.1 M ammonium sulfate ($(NH_4)_2SO_4$). A direct current (DC) bias voltage of 10 V was applied and maintained until the anodic graphite was completely consumed. Under the influence of the 10 V bias voltage, the bulk graphite rapidly expanded and was entirely consumed within a span of 1 hour. This process followed the optimized protocol reported in Ref. [17].

5.2 CG-GO films preparation

A solution containing GO in demineralized water was prepared with a concentration of 5 g·L^{-1}. Following this, the GO solution underwent a 20-minute ultrasonication process using an ultrasonic cleaner (SONOREX DIGITEC DT 510 H, 35 kHz, 9.7 L). The resulting homogenized solution was then deposited into a Petri dish and left to dry. The film produced in this manner was selected as the reference sample (S1). Further, CG solutions were prepared by dissolving sodium alginate (Sigma-Aldrich, China) at a concentration of 1.5 % and CG gum (predominantly κ with lesser amounts of λ CG, Sigma-Aldrich, USA) at a concentration of 1.5 % in separate beakers. Each solution was stirred using a magnetic stirrer until completely dissolved. Subsequently, the sodium alginate and CG gum solutions were mixed in a 40:60 ratio (CG:sodium alginate) and stirred for an additional hour. Meanwhile, a solution of GO was ultrasonicated for 20 minutes using an ultrasonic cleaner. Next, the sodium alginate and CG gum solutions were combined in the required amounts to achieve the desired concentrations of GO in the solution of 0.05 g·L^{-1} (S2) and 0.2 g·L^{-1} (S3). Additionally, 1 mL of glycerol was added as a plasticizer to 50 mL of the prepared solution. The resulting film-forming solution was then magnetically stirred for approximately 60 minutes to ensure thorough mixing. Finally, approximately 20 mL of the resulting solution was poured into individual Petri dishes and allowed to dry under natural conditions for about 48 hours.

When it comes to concentration, GO concentrations of 0.5 g·L^{-1} and higher are commonly employed in the literature [13, 16]. However, since our aim is to ensure even dispersion of GO flakes throughout the layer volume in our composite material, we initiated by assessing the transparency of the layers using Ultraviolet-visible (UV-Vis) spectroscopy at the wavelength of our laser (i.e., 1030 nm) to ascertain if uniform reduction could occur within the layer. We began the measurement at one-tenth of the aforementioned concentration, i.e., 0.05 g·L^{-1}, which yielded a transmittance value of 18.564 %. As we increased the GO concentration to 0.2 g·L^{-1}, the transmittance value dropped to 2.714 %. This significant drop in transmittance led us to conclude the experiment at this point; selecting these two GO concentrations for our work as a lower transmittance value would totally avoid rGO production by laser radiation through the whole film thickness.

5.3 Laser reduction of CG-GO films

We employed a high-energy industrial femtosecond laser, specifically the Onefive Origami XP-S, to process the CG-GO films. This laser model features a maximum repetition rate of 1 MHz, a center wavelength of 1030 nm, a pulse duration of fewer than 400 fs, an average output power of 5.1 W, and a spectral bandwidth of less than 5 nm. At the specified laser fluence setting of 50 mJ·cm^{-2}, which was determined through theoretical analysis [89], it was possible to reach an optimal level of fluence deemed fully sufficient for reducing the GO layer. For a visual representation of the experiment setup, please refer to Fig. 5.1.

Briefly, the processing of GO involved irradiation in a standard atmosphere. A series of reflecting mirrors directed the laser beam toward a scanning head. Subsequently, the beam traversed through the scanning head (intelliSCAN 14, SCANLAB), where two galvanometric mirrors facilitated swift changes in the beam's direction, allowing it to traverse across the film. An F-theta lens (f = 160 mm) was employed to focus the laser beam onto the surface of the CG-GO film contained within a plastic Petri dish. For controlling the laser scanning speed across the film, a speed of 1 m·s^{-1} was selected, regulated by the galvanometric mirrors. The film's surface underwent irradiation for one cycle using a specified raster-like pattern, with the distance between two adjacent lanes set at 0.03 mm. This method enabled the reduction of CG-GO films in accordance with the principles outlined in the theoretical section of this thesis.

5.4 Characterization of films

Various characterization techniques were employed to gain comprehensive insights into the characteristics of the produced films and evaluate their quality and performance for sustainable circuit applications. Scanning electron microscopy (SEM) and Energy-dispersive X-ray spectroscopy (EDS) were utilized to examine surface

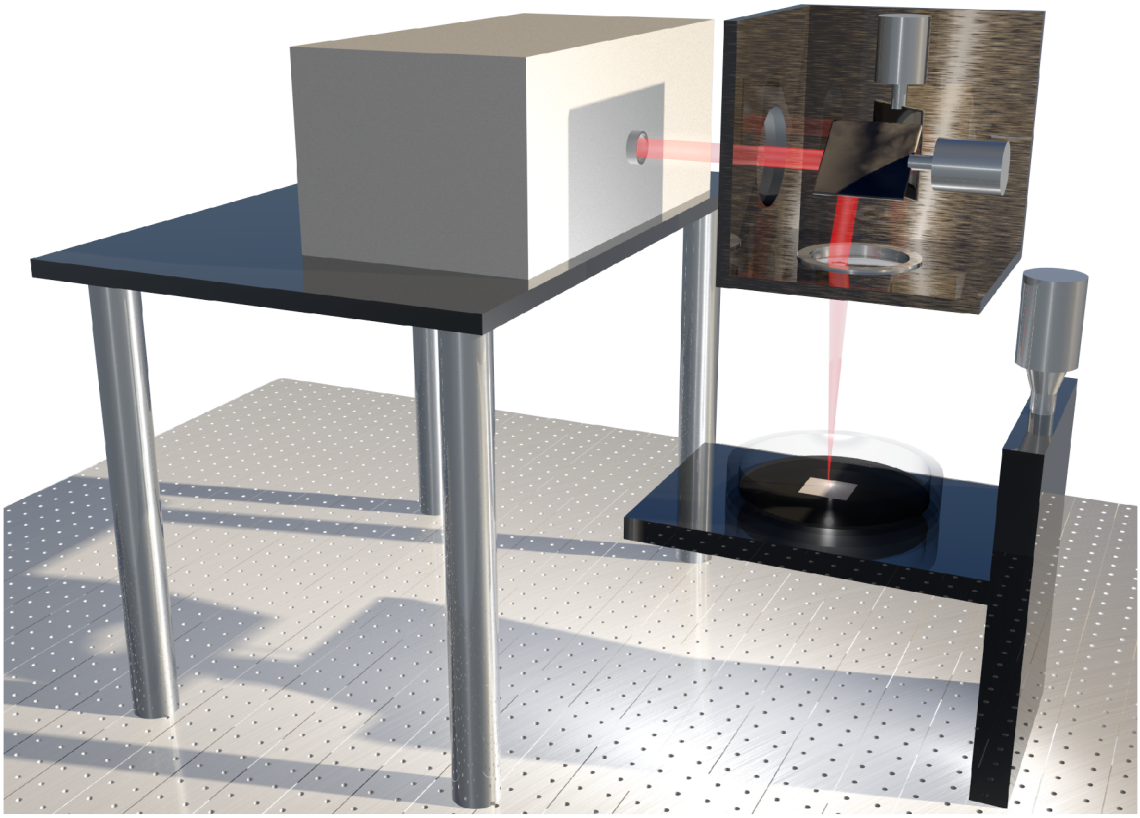

Figure 5.1: The experimental scheme of the CG-GO laser film reduction

features and element distribution within the samples, while Fourier transform infrared spectroscopy (FTIR) was employed to identify potential alterations in the polymer film structure induced by laser exposure. X-ray diffraction (XRD) and Raman spectroscopy were utilized to verify the reduction of GO to rGO. Additionally, the electrical properties of the developed films were analyzed.

For surface characterization, a high-performance Xe plasma-focused ion beam microscope, the Helios 5 PFIB CXe DualBeam (Thermo Scientific, USA), equipped with Oxford EDS and EBSD microanalytic detectors, was employed. The in-lens SE/BSE detector and in-column SE/BSE detector were predominantly utilized for sample analysis. Notably, the samples underwent no further specific modifications, such as plating, before analysis. They were mounted on a silicon wafer and inserted into the microscope chamber for observation. A low accelerating voltage, typically ranging from 0.5 to 1 kV, and a small working distance of 2 to 4.5 mm was applied to prevent undesired charging effects on the sample. These settings were carefully chosen to ensure accurate and reliable results during the analysis process. To determine film thickness, an ion beam was used to create a hole in the individual samples for cross-section analysis, which was only viable for sample S1. For CG-based samples, the thickness was assessed using the edges. Samples were examined at a 52° angle, and a cross-section correction was applied for thickness assessment. Additionally, an

EDS detector was utilized for surface analysis, requiring metallization of the samples with a 2 nm tungsten protection due to the higher accelerating voltage used.

The FTIR spectrometer employed in this study was the Nicolet iZ10 (Thermo Scientific, USA), equipped with a DTGS detector and an attenuated total reflectance (ATR) diamond crystal. Eight sample scans and 16 background scans were conducted to ensure data accuracy, with a resolution set at 4 cm^{-1} covering a spectral range from 4000 to 500 cm^{-1}. To optimize spectral data quality, the Happ-Genzel apodization function was applied, balancing spectral resolution and the size of spectral ripples. Corrections for atmospheric interference and baseline variations were also implemented.

The Raman analysis was performed using the DXR Raman microscope (Thermo Scientific, USA) equipped with an Olympus MPlan 50x objective. The examination utilized the following parameters: an excitation laser wavelength of 532 nm, a laser power of 5 mW, a 50 μm aperture, a FullRange grating with 900 scratches/mm, 150 exposures, an exposure time of 1 second, and a spectral range spanning from 3500 to 100 cm^{-1}. Additionally, baseline correction techniques were applied to refine the spectra, enhancing the quality and accuracy of the Raman measurements. The crystallographic structure of the specimens was assessed using X-ray diffraction in powder form with a diffractometer Miniflex 600 (Rigaku, Japan), employing Co Kα1 radiation ($\lambda = 1.788$ Å) within a 2θ angle range of 3–90° at a scan rate of $1°{\cdot}min^{-1}$. In order to conduct a more thorough examination of the XRD findings, a Rietveld refinement analysis was carried out using the MAUD software [96]. Resistance measurements were performed using the GOM-805 DC Milliohm Meter. This versatile multimeter enables the measurement of resistance from 0.05 Ω to 5 MΩ, with a resolution of 1 $\mu\Omega$, a test current of 1 A, and an accuracy level of 0.05 %. A specimen measuring 2.25 cm^2 in area was extracted from each film and carefully positioned on a glass surface to avoid any interference with the conductive properties of the underlying substrate material. Subsequently, a set of electrodes were precisely positioned at a distance of 1.5 cm from each other, enabling the measurement of the resistance exhibited by the film.

6 Results and discussion

6.1 SEM

The surface morphology of developed films was determined by SEM. Sample images illustrating the progressive increase in detail regarding the most intriguing morphological characteristics of individual specimens are available in Fig. 6.1.

Upon closer examination of film S1, an array of minute irregularities, such as wrinkles and corrugations, adorn its surface, likely stemming from the film's preparation process. This involved dispersing GO flakes, obtained through electrochemical exfoliation, in demineralized water, followed by homogenization and subsequent drying. Such a process may have led to variations in rotations or partial unevenness of the flakes. Subsequent irradiation (referred to as S1T) of the surface with a laser resulted in more pronounced wrinkling, along with the emergence of uneven pores and detached layers. These structural alterations may arise from the elimination of oxygen-containing groups and weakly bonded carbon atoms during the laser-induced reduction process, thereby increasing the defect density. Alternatively, the cumulative effect of pulsed laser exposure, generating heat, could initiate pyrolysis and the subsequent removal of volatile components. Upon closer scrutiny of the S1T structure, certain features resembling LIPSS are discernible on the surface, likely formed by utilizing a laser fluence of 50 $\mathrm{mJ{\cdot}cm^{-2}}$. Unfortunately, these structures appear to have been compromised. Upon further magnification, nanoparticles (NPs) ranging from 20-40 nm can be identified dispersed across the surface of S1T. These NPs likely represent a single atomic layer of carbon NPs formed through a sublimation reaction followed by rapid condensation, which is the typical carbon NPs formation process when employing laser ablation [97].

When GO is introduced into the polymer matrix, the structure undergoes a fascinating transformation. The increase in GO dispersion leads to amplified surface irregularities, as seen in the comparison of samples S2 and S3, with S2 displaying a relatively smoother surface. After irradiation, a noticeable surface expansion occurs, attributed to the creation of bubbles with varying sizes and shapes. Upon closer inspection of sample S2T, the formation of notably larger bubbles is more prevalent compared to the S3T sample. A significant distinction also arises in the development of pores, with S2T showing a minimal presence of pores while the S3T sample showcases a pervasive distribution of pores throughout the surface.

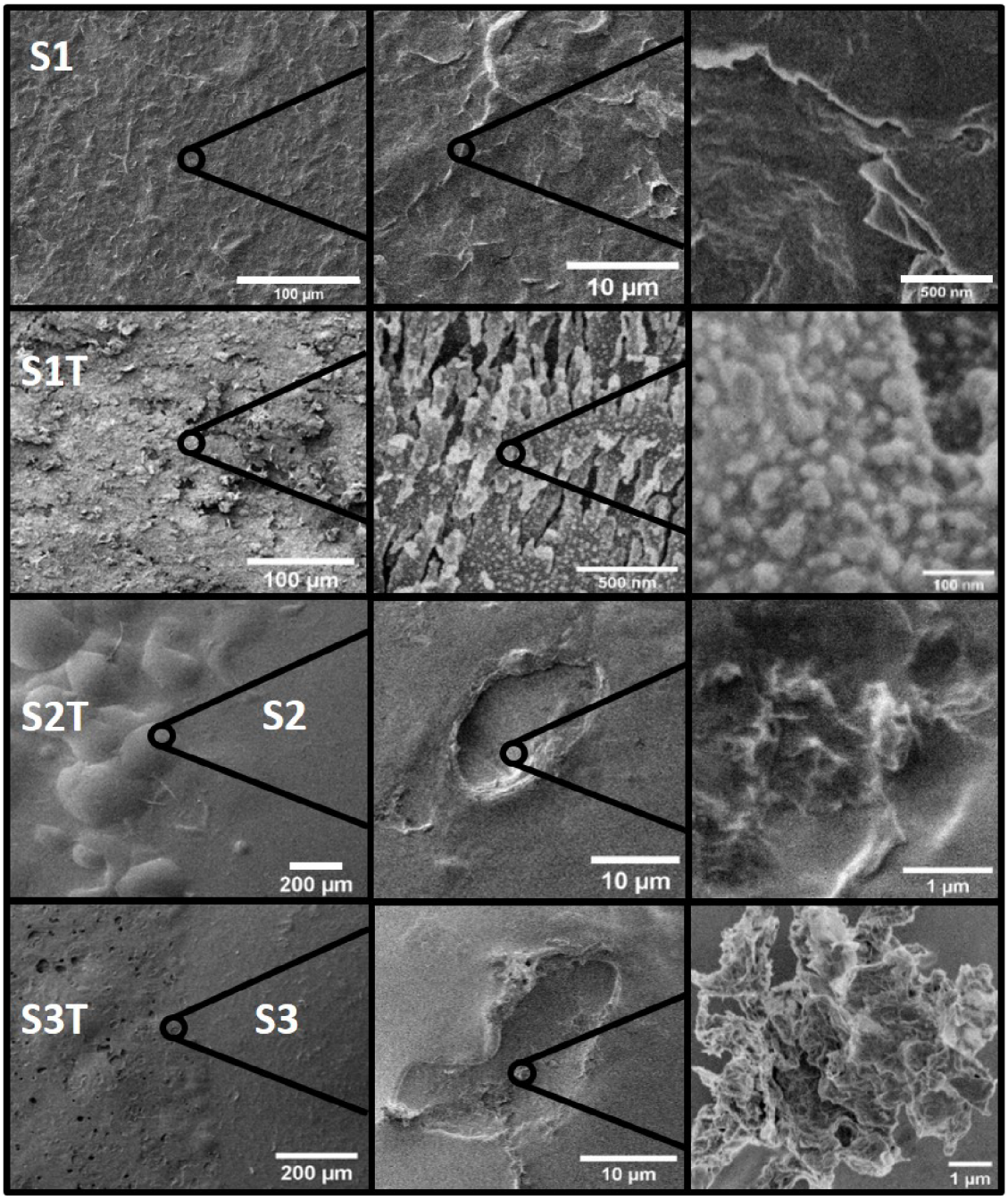

Figure 6.1: Representative SEM images of developed films

It seems that at lower concentrations of GO in the samples, the formation of bubbles and pores within the polymer matrix is sporadic; however, as the dispersion of GO increases, the emergence of pores becomes more pronounced. Within these pores, structures reminiscent of those found in the S1T sample are discerned, albeit not entirely identical. This inconsistency may be attributed to the differences in the level of reduction of GO flakes within the polymer matrix, given that a portion of the laser energy is dissipated as it traverses through the polymer material.

6.1.1 Thickness measurement

Thanks to the utilization of an ion beam and the ability to tilt the sample within the SEM chamber, it was possible to conduct precise measurements of the thicknesses of distinct layers using cross-sectional analysis. To find the thickness of films, 10 values of thickness for each sample were measured using the software ImageJ. The SEM images, accompanied by tables presenting the results of the arithmetic mean ($\overline{x}$) and sample standard deviation (s) for the thickness of individual films, as well as the difference in thickness between the irradiated and non-irradiated sections of the layer, are depicted in Fig. 6.2.

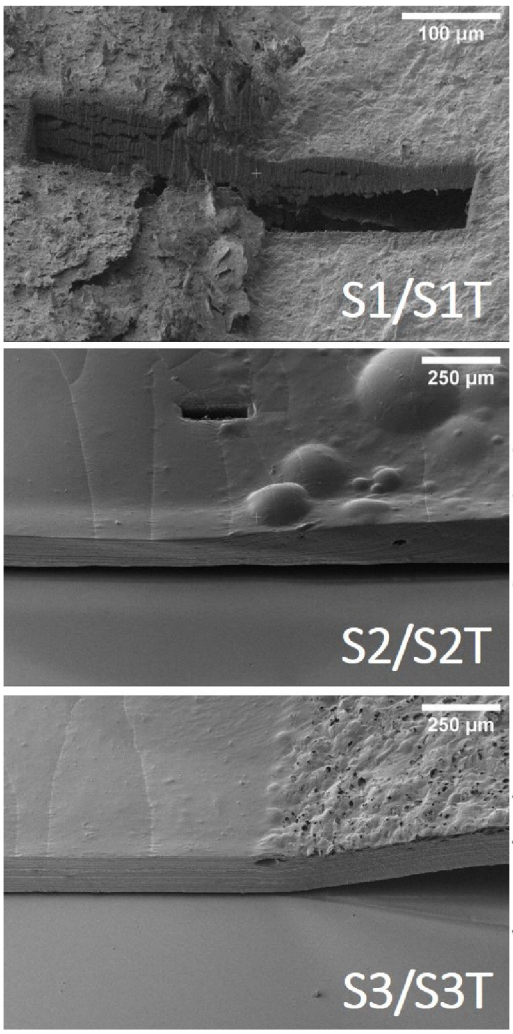

Sample	$S1$	$S1T$	$\delta(S1/S1T)$
$\overline{x}$ (μm)	25.19	49.80	24.61
s (μm)	2.37	3.59	-

Sample	$S2$	$S2T$	$\delta(S2/S2T)$
$\overline{x}$ (μm)	89.34	116.27	26.93
s (μm)	4.17	12.21	-

Sample	$S3$	$S3T$	$\delta(S3/S3T)$
$\overline{x}$ (μm)	110.42	116.48	6.06
s (μm)	0.98	4.39	-

Figure 6.2: Sample SEM images with the corresponding values of the arithmetic mean ($\overline{x}$) and sample standard deviation (s) of the thickness of the individual layers located in the table

Regarding sample S1, the average layer thickness was found to be 25.19 ± 2.37 μm. It was anticipated that there would be a slight reduction in material post the application of laser radiation. Surprisingly, for the S1T sample, the layer thickness nearly doubled, measuring at 49.80 ± 3.59 μm. This is likely associated with the creation of numerous vertical nano-sheets, as demonstrated in the investigation referenced in Ref. [89], which utilized femtosecond laser irradiation at a fluence of around 40 mJ/cm^2.

CG matrix films, in general, exhibit considerably greater thickness values when compared to S1. The SEM image illustrates the boundary between S2 and S2T, revealing a hole created by an ion beam that remains due to an unsuccessful endeavor to gauge the disparity in thickness between these particular specimens. This occurrence can be attributed to the collapse of bubbles that were generated while subjecting this specific sample type to irradiation. Consequently, the layer thickness was gauged from the boundaries, resulting in measurements of 89.34 ± 4.17 μm for S2 and 116.27 ± 12.21 μm for S2T. Here, once more, a substantial augmentation is observed in the irradiated part of the sample, attributed to polymer swelling. The bubbles' sizes are notably larger in S2T compared to S3T, as highlighted by the sample's standard deviations, with S2T showing an almost threefold increase in deviation. This signifies a greater discrepancy in the irregularities present on the surface of this particular sample. The thickness of S3 was established at 110.42 ± 0.98 μm, marking it as the largest among the pristine samples. Conversely for S3, the smallest increment was a mere 6.06 μm, predominantly caused by the numerous open pores on the film's surface.

6.2 EDS

The incorporation of the EDS detector within the utilized SEM device enabled the expansion of the research through EDS line and mapping analysis for determining the elemental composition of the developed films. Line microanalysis was conducted along a specific line on the sample's surface, facilitating the acquisition of both quantitative and qualitative data, including the element concentration distribution along the chosen line. The resultant spectrum, with the corresponding marked line indicating the analysis location, is visible in Fig. 6.3. Analysis of the EDX spectrum reveals the presence of carbon and oxygen in both the film's non-irradiated (S1) and irradiated (S1T) sections. Notably, the reduction process resulted in a 10 wt% reduction in the surface atomic percentage of oxygen, while the C/O ratio increased from 2.6 to 11.77 for GO and rGO, respectively. This signifies a notably higher oxygen content in the pristine GO than rGO, aligning with the hypothesis presented in this work's theoretical part.

Additionally, surface microanalysis of a specific area of the sample was carried out to determine the element concentration distribution. The resultant EDS mapping, presented in Fig. 6.4, illustrating oxygen in green and carbon in red, allows clear

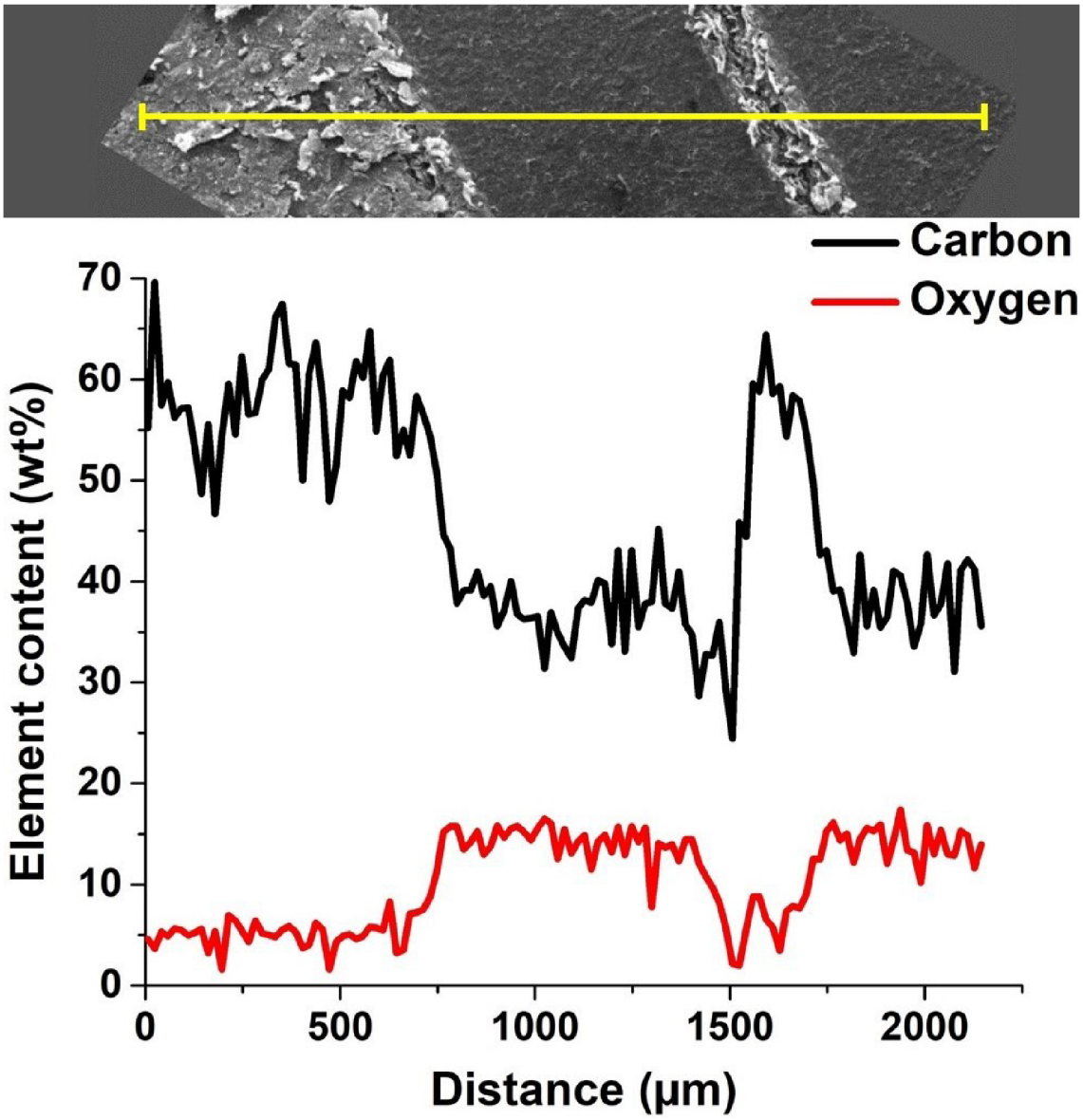

Figure 6.3: EDS line analysis through the non-irradiated (S1) and irradiated (S1T) part of pristine GO

distinguishing between the non-irradiated (S1) and irradiated (S1T) regions of the film. The S1 area exhibits a higher oxygen content due to the presence of diverse oxygen groups in pure GO. Upon exposure to laser radiation, a significant decrease in the green color is observed in the S1T region, indicating the removal of most oxygen groups. Overall, the outcomes of the EDS analyses confirm the successful reduction of GO to rGO utilizing the specified laser parameters. Note that no EDS analysis was conducted on the films containing the polymer, as its high carbon content could mask the signals of carbon and oxygen resulting from the reduction of GO. This masking effect could potentially lead to misinterpretations of the EDS data.

Figure 6.4: EDS map analysis through the non-irradiated (S1) and irradiated (S1T) part of pristine GO

6.3 FTIR

Moreover, an analysis of the films was carried out through the utilization of infrared spectroscopy with Fourier transformation. The primary objective of this analysis was to determine whether the specific laser parameters employed for the reduction process could potentially cause any deterioration in the polymer matrix. Upon careful examination of the graph presented (Fig. 6.5), it is evident that both sample S2 and sample S3 exhibit a remarkable similarity between the results obtained before irradiation (depicted in the black spectrum) and those after irradiation (illustrated in the red spectrum). Consequently, it can be deduced that the application of laser radiation utilizing the aforementioned parameters does not induce any form of degradation or alterations in the polymer's structural composition.

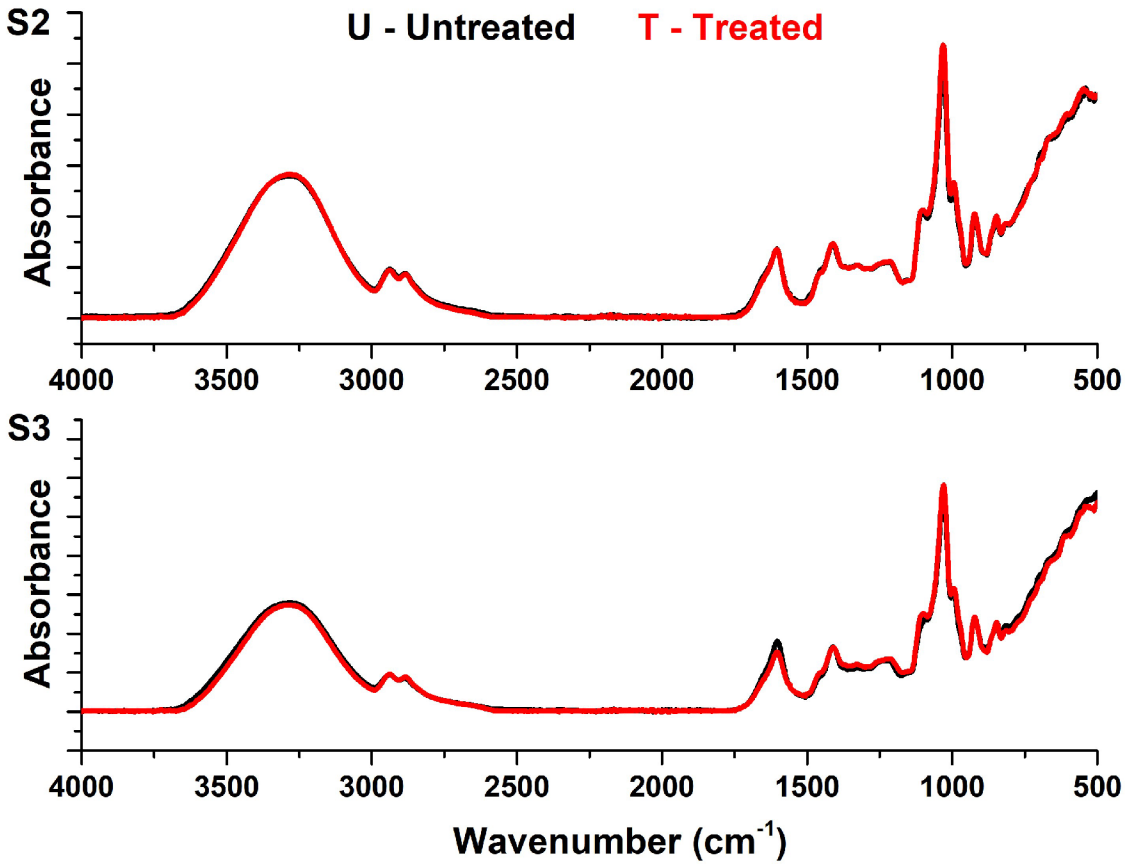

Figure 6.5: FTIR analysis of CG-based films, where non-irradiated samples are labeled in black and irradiated ones in red

6.4 Raman

To ratify the data extracted in the EDS section, we conducted an analysis of the films by examining the Raman spectra within the wave number range of 100 to 3500 cm^{-1}. This approach is well-established as a straightforward and non-intrusive method for examining carbon structures. Carbon materials typically exhibit three distinctive bands, as illustrated on the graph (Fig. 6.6). The D band, observed at approximately 1346 cm^{-1} in this context, indicates defects in the graphene structure. The G band, detected around 1587 cm^{-1}, corresponds to the sp^2 vibrations of atoms. Finally, the 2D band, appearing at approximately 2694 cm^{-1}, reflects the stacking arrangement of multilayer graphene atoms.

Of particular interest to us is the ratio of the D/G band intensities, widely employed to assess the reduction level of GO. A smaller ratio indicates a higher degree of reduction [16, 98]. The specific ratios displayed on the left side of the chart evidence that there is a decrease in the intensity of the D/G band after the sample is irradiated in all instances, indicating a consistent reduction across the board. Notably, the most significant reduction was observed in sample S1, which consisted solely of

GO, with intensity ratios dropping from 1.03 to 0.23 for S1 and S1T, respectively.

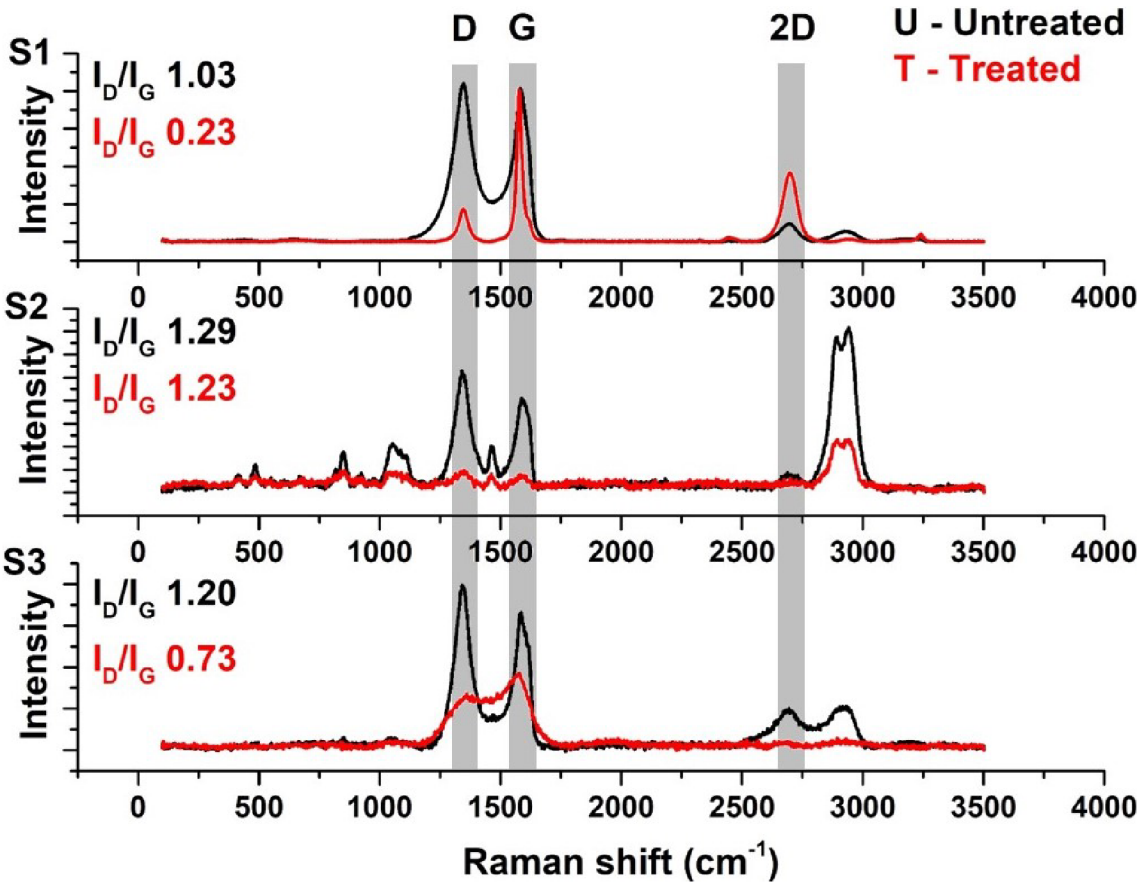

Figure 6.6: Raman spectra of created films, where non-irradiated samples are marked in black and irradiated ones in red

For sample S2, there is a minimal decrease in the intensity ratio, specifically 1.29 for the non-irradiated film and 1.23 for the irradiated film. This observation is likely attributed to the appearance of the sample's surface, which predominantly consisted of a swollen semi-layer with really low amount of open holes containing rGO flakes. As a result, the ratio of D/G band intensities in both samples was nearly identical. This deduction is further reinforced by the findings of sample S3, where the intensity ratio decreased from 1.20 to 0.73 for S3 and S3T, respectively, indicating more favorable outcomes in terms of reduction. Despite numerous bubbles on the surface of this sample, in contrast to sample S2, a significant number of holes filled with rGO flakes could be found.

6.5 XRD

Further investigation into the reduction and determination of crystallinity and phase purity of the synthesized samples was carried out through XRD analysis. The XRD patterns corresponding to all the examined samples can be observed in Fig. 6.7. For sample S1, it becomes apparent that there are two distinct peaks present at 2θ angles of 11.74° and 26.36°, with the former peak being characteristic of GO and the latter associated with graphite [99]. Following the exposure to laser radiation, there is a noticeable decrease in the intensity of the peak at 2θ angles of 11.74°, accompanied by a shift towards higher 2θ angles, specifically converging to the value of 14.42°. This decline in intensity and shift towards higher angles is interpreted as a clear indication of the GO reduction process taking place [99, 100]. Conversely, in samples containing CG, there are no significant variances readily apparent to the naked eye. Across the XRD pattern of all the samples, two broad peaks emerge at approximately $2\theta = 21°$ and 35°. These observed peaks align closely with the characteristic values associated with κ-CG [101, 102], which serves as the predominant constituent in the construction of the films. The presence of these two broad peaks serves as a strong indicator of the amorphous nature of these films.

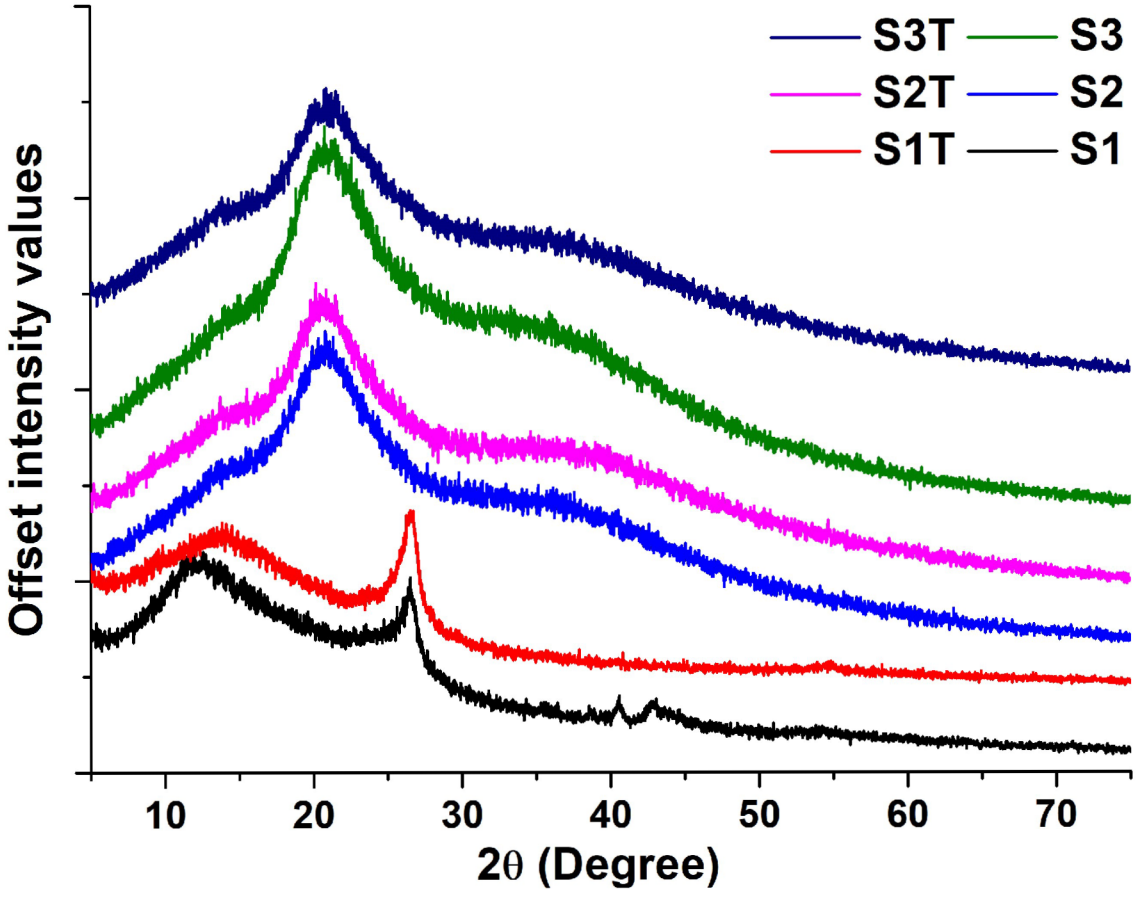

Figure 6.7: Representative XRD patterns of created films

Upon closer examination of the individual XRD patterns, it becomes apparent that distinct trends can be observed in the curves within the range of 7° to 12°. Notably, the irradiated samples, specifically S1T, S2T, and S3T, exhibit a more subdued trend compared to the non-irradiated counterparts. To facilitate comprehensive comparison across all samples, the intensity of the minimum at 2θ angle 7.35° and the intensity of the maximum at 2θ angle 11.24° were initially determined. These specific values were carefully selected to ensure an adequate separation enabling the trend of the curve to be discerned accurately. Subsequently, the ratio of these two values (I(min)/I(max)) was calculated, yielding ratio values of 0.701, 0.817, 0.769, 0.769, 0.704, and 0.768 for S1, S1T, S2, S2T, S3, and S3T respectively. Analysis of these results reveals that, except for samples S2 and S2T showing negligible variation in the ratio value, the irradiated samples exhibit higher ratio values compared to the non-irradiated samples. This observation is further supported by the gentler slope of the curves in the irradiated samples. The most substantial difference in intensity ratios is evident in samples S1 and S1T, where the ratio increased from 0.701 to 0.817, indicating a decrease in the intensity of the characteristic GO peak around 11°, thereby signifying reduction as mentioned earlier. Similarly, a comparable trend is observed in S3 and S3T, albeit with slightly lower intensity ratios, suggesting reduction albeit to a lesser extent likely due to laser fluence losses in the polymer matrix. Furthermore, these findings align with the outcomes of Raman spectroscopy, where the intensity ratio of the D/G bands was assessed, showcasing the highest reduction degree in S1, followed by S3 and S2, with S2 displaying nearly identical intensity ratio values, similar to XRD.

To delve further into the characterization of crystallinity and phase purity, the Rietveld refinement method was employed. The utilization of the MAUD software, an acronym for Materials Analysis Using Diffraction, allowed the execution of this analysis. This software, available at no cost, enables the examination of diffraction data through a unified Rietveld approach [96]. The refinement process was exclusively conducted on samples S1 and S1T due to the predominance of carrageenan spectrum in the other samples, obscuring the distinctive peaks associated with GO. The Crystallography Open Database (COD) was utilized to identify a maximum number of matching Crystallographic Information Files (CIFs) in the context of this study. Given the nature of this being an unpaid resource, the CIF 4131687, which pertains to graphene nanoribbons with a monoclinic space group ($P2_1/c$), and CIF 1200017, corresponding to graphite with a hexagonal space group ($P6_3mc$), were deemed sufficient for the investigation. The analysis entailed the processing of a spectrum detailing crystal structure data, along with a viable Rietveld refinement assessment featuring values documented in a table, as illustrated in Fig. 6.8.

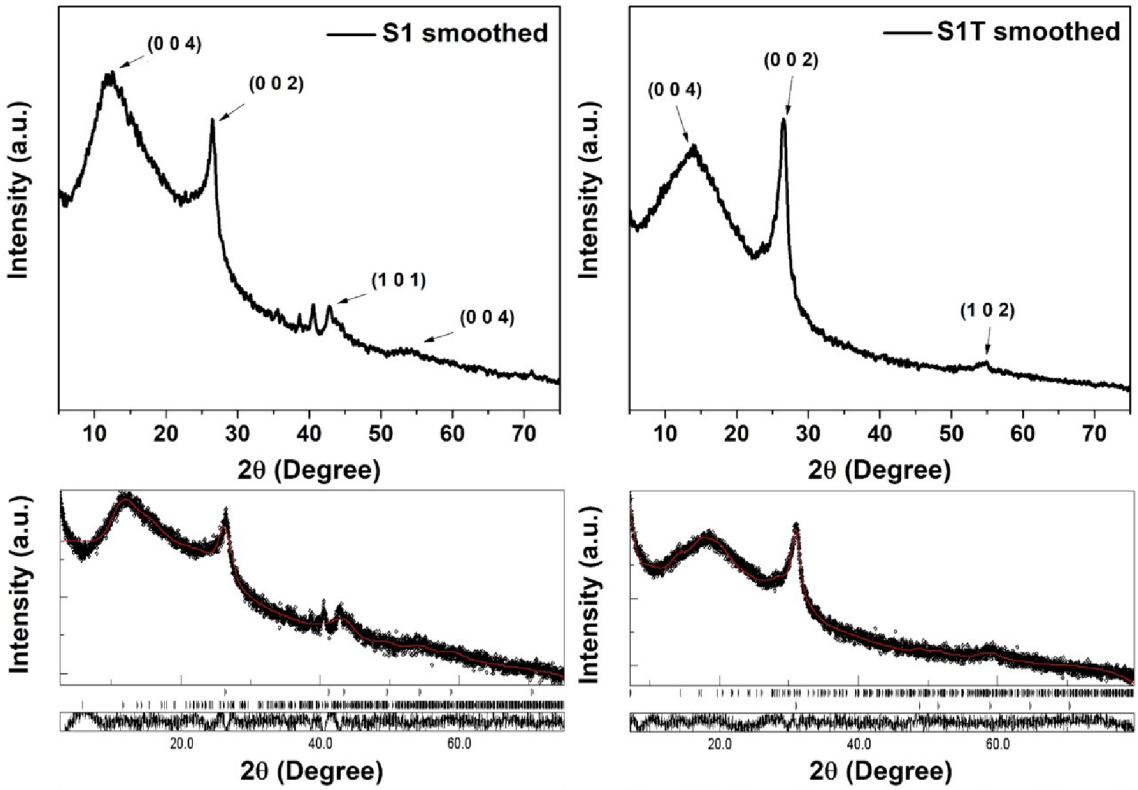

Crystal family	$C_{20}H_{14}O_2$	C
S1 (wt%)	78.1	21.9
a (Å)	6.50	2.53
b (Å)	5.22	-
c (Å)	34.17	6.76

Crystal family	$C_{20}H_{14}O_2$	C
S1T (wt%)	74.1	25.9
a (Å)	5.25	2.15
b (Å)	4.12	-
c (Å)	24.92	5.76

Figure 6.8: XRD spectra of samples S1 and S1T revealing their crystal structure (upper section of the figure) and their corresponding Rietveld refinement analysis, along with a pair of tables summarizing the results (lower part of the figure). Note that the accuracy of the Rietveld refinement is supported by an R_{wp} (%) of 7.234 for S1, and 6.505 for S1T.

The outcomes of the Rietveld refinement evaluation reveal that sample S1 comprises 78.1 wt% of $C_{20}H_{14}O_2$ with monoclinic lattice parameters established as a = 6.50 Å, b = 5.22 Å, c = 34.17 Å, and 21.9 wt% of C with hexagonal lattice parameters a = 2.53 Å, c = 6.76 Å. Following the irradiation of sample S1 to create S1T, there are alterations in these parameters. Sample S1T consists of 74.1 wt% $C_{20}H_{14}O_2$ with monoclinic crystal lattice parameters determined as a = 5.25 Å, b = 4.12 Å, c = 24.92 Å, and additionally 25.9 wt% of C with hexagonal lattice parameters a = 2.15 Å, c = 5.76 Å. As you can see, all parameters exhibit a decrease in their values, suggesting a contraction of the crystallographic lattice. Despite the smaller size of oxygen compared to a carbon atom, owing to the enhanced effective nuclear charge of the atom's nucleus, the removal of oxygen through the reduction process results in a contraction of the crystallographic lattice. On top of this, the XRD of

S1 shows two significant diffraction lines at 2θ angles of 11.74° and 26.36° related to reflections from (0 0 4) and (0 0 2) planes. The distance between GO layers for 2θ = 11.74° reflection is measured to be 7.53 Å, using Bragg's equation. The d-spacing of GO is larger than that of natural graphite (approximately 3.3 Å) which is due to the presence of oxygen-containing functional groups between the GO planes. In the counterpart, the XRD pattern of S1T shows two significant peaks again but in this case, at 2θ = 14.42° belongs to the (0 0 4) plane, and at 2θ = 27.321° belongs to (0 0 2). The measured d-spacing of S1T is about 6.13 Å which is less than the S1 d-spacing (7.53 Å). This can be attributed to the removal of functional groups and water molecules from GO after conversion to rGO.

6.6 Conductivity determination

A fundamental requirement for the practical application of these films in the field of electronics is low electrical resistivity, which means a high level of conductivity. This characteristic is crucial as it demonstrates the material's ability to impede the flow of electric current. This value allows for a direct comparison of the resistance levels among various types of conductors under the same temperature conditions, irrespective of their dimensions. In essence, higher resistivity indicates a higher resistance, while lower resistivity signifies a lower resistance level. Consequently, the resistance of each film was assessed, and the outcomes of this evaluation are detailed in Tab. 6.1.

Sample	$S1(\Omega)$	$S1T(\Omega)$	$S2(M\Omega)$	$S2T(M\Omega)$	$S3(M\Omega)$	$S3T(M\Omega)$
$\overline{x}$	196.41	6.12	1.09	0.24	0.69	0.33
s	65.20	0.66	0.19	0.04	0.14	0.03

Table 6.1: Arithmetic mean ($\overline{x}$) of measured resistance of individual films with sample standard deviation (s)

Subsequently, these values were substituted into the relation for resistivity (Eq. 6.1):

$$\rho = \frac{R \cdot A}{L}, \tag{6.1}$$

where ρ is the proportional constant known as resistivity ($\Omega{\cdot}m$), R is the resistance (Ω), L is the length (m) and A is the area (m^2).

The values obtained for resistivity, along with conductivity (σ), which represents the reciprocal of resistivity (as indicated in Eq. 6.2), are displayed in Tab. 6.1. Analysis of film S1 revealed a conductivity of $3.39{\cdot}10^{-3}\ S \cdot cm^{-1}$. The considerably high standard deviation, in the case of resistance of the sample, is likely attributed to the uneven distribution of the GO flakes within the film. A comparative analysis between samples S1 and S1T showcases a remarkable two-order of magnitude increase

in conductivity, highlighting the remarkable effectiveness of the laser parameters selected for the study.

On the other hand, films incorporating a CG matrix display conductivity levels indicative of decent insulating properties. Sample S2 exhibited a conductivity of $0.61{\cdot}10^{-6}\ S{\cdot}cm^{-1}$, a value four orders of magnitude higher than that of S1. Notably, as the concentration of GO within the polymer matrix increases, there is a corresponding increase in film conductivity, exemplified by sample S3 with a conductivity of $0.97{\cdot}10^{-6}\ S \cdot cm^{-1}$. While the increase in the S2 sample's conductivity was not conclusively demonstrated in the additional analyses, there is evidence of a change occurring, as the conductivity of the film increased to around one-fourth of its initial value post-irradiation, specifically $2.78{\cdot}10^{-6}\ S{\cdot}cm^{-1}$. These results suggest that some transformation or modification is indeed taking place within the S2 sample following the irradiation process. Similarly, an increase in conductivity is noted for S3T, albeit to a lesser extent at $2.02{\cdot}10^{-6}\ S \cdot cm^{-1}$.

It is noteworthy that the S2T sample displays higher conductivity compared to the S3T sample, despite the latter containing a notably higher concentration of GO. This phenomenon could potentially be attributed to the high porosity observed in the SEM images of the S3T sample, as conductivity tends to decrease with the presence of highly porous materials. Despite this, the conductivity of S3T is higher than that of non-irradiated S3, hinting at a partial reduction of the film being a contributing factor. The laser parameters utilized in the study demonstrate the feasibility of the GO reduction process, even when GO is dispersed within the polymer matrix. However, the conductivity values of such films are deemed too low for practical applications in flexible electronics.

$$\sigma = \frac{1}{\rho} = \frac{L}{R \cdot A} \tag{6.2}$$

Sample	$S1$	$S1T$	$S2$	$S2T$	$S3$	$S3T$
$\rho\ (\Omega \cdot cm)$	294.62	9.17	$1.64{\cdot}10^{6}$	$0.36{\cdot}10^{6}$	$1.04{\cdot}10^{6}$	$0.50{\cdot}10^{6}$
$\sigma\ (S \cdot cm^{-1})$	$3.39{\cdot}10^{-3}$	0.11	$0.61{\cdot}10^{-6}$	$2.78{\cdot}10^{-6}$	$0.97{\cdot}10^{-6}$	$2.02{\cdot}10^{-6}$

Table 6.2: Table of resulting values of resistivity (ρ) and conductivity (σ)

6.7 Flexibility

Good flexibility is another crucial characteristic for the successful application of the developed films within the realm of flexible electronics, as it directly impacts their performance and durability. Consequently, in order to assess the flexibility of the individual films, two distinct bending tests were conducted to evaluate their mechanical behavior under different conditions. The first test involved a simple bending process, where both ends of the film were gradually brought closer to each other to

observe its response to such deformation. In the second test, the film was subjected to a more complex twisting motion, ultimately forming the shape of a cylinder to ascertain its ability to withstand varying degrees of bending. The detailed results and findings of these bending tests are visually represented in Fig. 6.9.

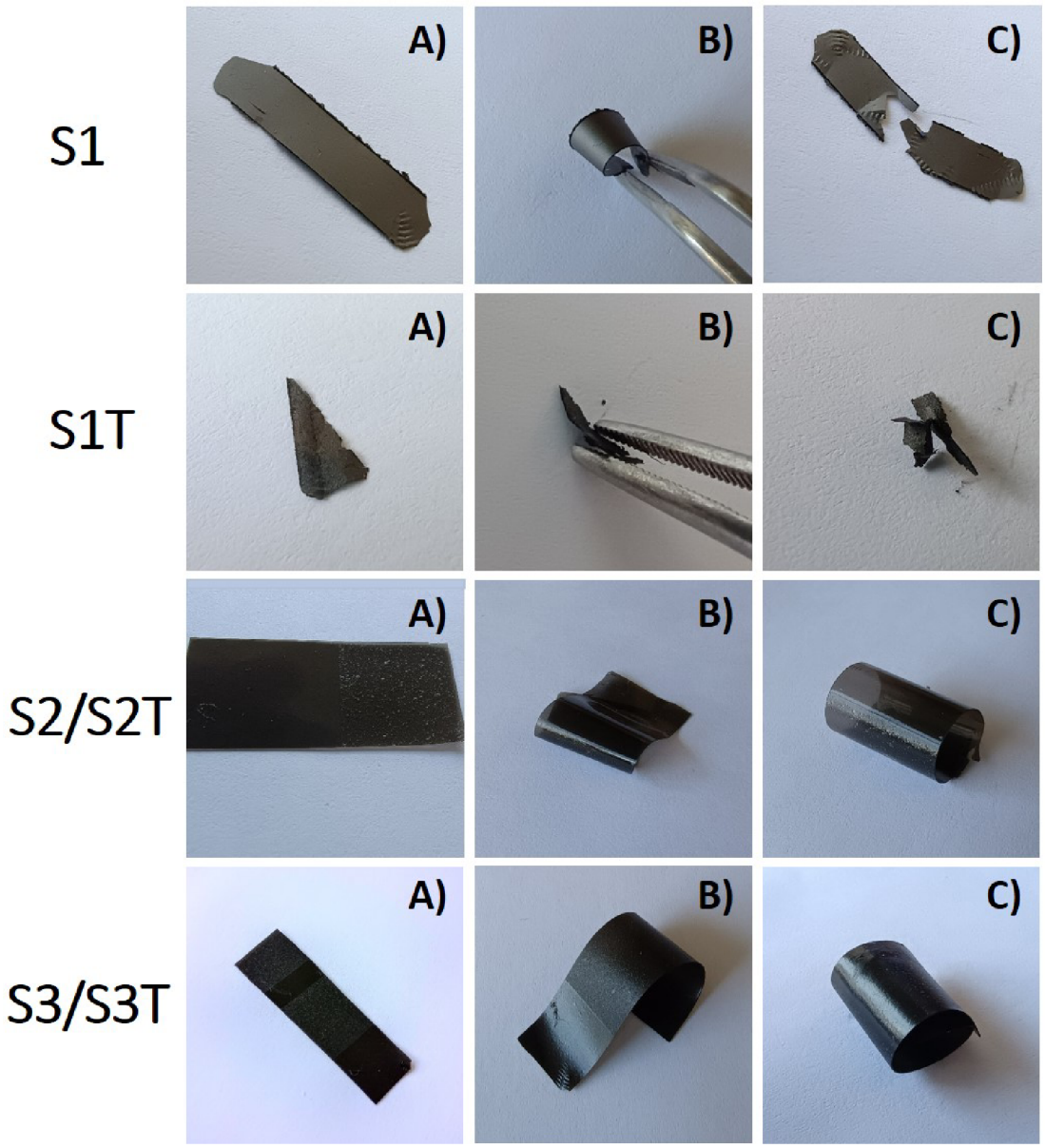

Figure 6.9: Flexibility test of developed films showing A) test piece, B) simple bending, and C) twisting of individual films

For sample S1, it was feasible to achieve a certain degree of bending; however, this flexibility was limited in scope. Attempting to twist the film resulted in its cracking and breaking into two distinct fragments. The sample S1T, on the other hand, presented challenges in isolation on a large scale due to its exceptionally tight adhesion

to the substrate, thus indicating its inherent lack of flexibility. Any effort to bend this film led to irreversible deformation, causing it to disintegrate into smaller components. Conversely, the remaining samples S2, S2T, S3, and S3T, all possessing a base of CG, exhibited significantly better outcomes in terms of flexibility, as expected. The flexibility of these films allowed for various bending configurations and reversible twisting, such as forming them into a cylindrical shape, as illustrated in Fig. 6.9. These results underscore the pivotal role played by the polymer substrate or matrix in the development of flexible circuits. Despite the notably lower resistivity values (indicative of higher conductivity) displayed by samples S1 and S1T, their flexibility remained notably poor, with S1T essentially lacking any semblance of flexibility. In contrast, the CG matrix emerges as a promising foundation for the fabrication of flexible circuits.

7 Conclusion

In the current diploma thesis, highly sustainable composite materials were developed by combining a carrageenan matrix with different concentrations of GO dispersion. These materials underwent a subsequent treatment involving exposure to femtosecond laser radiation to effectively reduce the GO flakes distributed within the polymer matrix structure. Unlike conventional practices of depositing GO on flexible substrates like dip-coating, the focus here was on achieving irradiation of GO flakes dispersed throughout the entire volume of the polymer structure, setting this study apart from existing methodologies. The latter methods are known for being laborious and costly compared to the direct integration of GO into a polymer matrix, which motivated our experimental approach. Moreover, the selection of a carrageenan matrix as the fundamental component for these composite films represents another distinctive aspect of this research. The resultant films exhibited varied morphologies, degree of reduction, and levels of conductivity, all influenced by factors such as the concentration of GO flakes and the presence of the polymer matrix.

From a morphological perspective, several significant variances were observed in all three samples subsequent to their exposure to laser irradiation. The S1T sample exhibited substantial wrinkling on its surface, along with numerous uneven pores and detached layers. Upon closer inspection, structures resembling LIPSS were visible, albeit in a damaged state. Further magnification revealed the presence of carbon particles forming a monoatomic layer across the entire surface of S1T. In contrast, the surfaces of S2T and S3T displayed a considerable number of bubbles that formed during the irradiation of the polymer matrix. Notably, S2T featured larger unopened bubbles, whereas in S3T, the bubbles were smaller and open, resembling a multitude of pores. Within these pores, rGO-like structures were identified, suggesting some degree of reduction had taken place.

Similar findings were derived from the analyses conducted using Raman spectroscopy and XRD, primarily aimed at assessing the extent of reduction. As anticipated, the most substantial reduction was observed in sample S1T, which lacked a polymer matrix, followed by samples S3T and S2T. The reduction level decreased in samples S3T and S2T due to the lower amount of GO. This ranking was determined based on the ratios of intensity between the D/G bands in the Raman spectrum and the minimum and maximum intensities in the 2θ angle range of 7-12° in the XRD spectrum.

Moreover, films containing a polymer matrix demonstrated markedly superior properties in terms of flexibility compared to films lacking a polymer base, which essentially disintegrated under various bending attempts. Conversely, the former films exhibited the ability to be twisted and bent in any manner, highlighting exceptional flexibility attributes suitable for applications in flexible circuits. Subsequent research endeavors will focus, among others, more on evaluating the mechanical and strength characteristics of films based on carrageenan. Conversely, films utilizing a carrageenan matrix exhibited conductivity values up to four orders of magnitude lower than films devoid of a polymer base. For instance, in the case of sample S1, the conductivity increased from $3.39{\cdot}10^{-3}\ S \cdot cm^{-1}$ to a mere $0.11\ S \cdot cm^{-1}$, representing a two-order-of-magnitude increase. Meanwhile, for samples S2 and S3, the conductivity registered in the range of $10^{-6}\ S \cdot cm^{-1}$, with the conductivity growing up, as expected, with an increase in the concentration of GO in the polymer. Upon irradiation of samples S2 and S3, the conductivity increased, albeit still fluctuating in the hundreds of $10^{-5}\ S \cdot cm^{-1}$ range, indicative of insulating properties. It is important to highlight that the S3T sample displayed lower conductivity values than the S2T sample, despite containing a notably higher volume fraction of GO. This particular observation is linked to the morphology of the S3T sample, as previously discussed.

The remarkable observations made should be duly noted that despite the increase in conductivity resulting from the reduction process, the value obtained is not nearly adequate for the practical applications of these films within the field of flexible circuits. The findings clearly indicate that the issue lies precisely within the polymer matrix, which remains relatively unaffected during irradiation. While it is feasible to expose and partially reduce some GO flakes, this only leads to a minimal increase in conductivity. Furthermore, the concept of establishing conductive pathways within the polymer matrix appears almost unattainable due to the formation of bubbles of varying sizes on the film's surface during irradiation. The primary advantage of the selected methodology lies in the facile production process and the favorable flexible properties derived from the carrageenan base.

On the other hand, these findings provide a pathway for new perspectives on the entire topic and potential enhancements to the current combination of these versatile composite films. A prospective solution that we intend to explore in the future involves depositing GO onto the carrageenan polymer layer, perhaps through dip-coating, implementing localized micropatterning, simultaneous reduction of specific sections using laser technology, and subsequently enveloping the structure with an additional protective polymer layer. This approach aims to fabricate an enhanced flexible circuit, blending excellent flexibility from the carrageenan-based polymeric substrate with adequate conductivity from the rGO pathways.

References

1. LEE, Jaehong; LLERENA ZAMBRANO, Byron; WOO, Janghoon; YOON, Kukro; LEE, Taeyoon. Recent Advances in 1D Stretchable Electrodes and Devices for Textile and Wearable Electronics: Materials, Fabrications, and Applications. *Advanced Materials* [online]. 2020, vol. 32, no. 5, p. 1902532 [visited on 2024-05-10]. ISSN 0935-9648, ISSN 1521-4095. Available from DOI: 10.1002/adma.201902532.

2. HASSAN, Gul; BAE, Jinho; LEE, Chong Hyun. Ink-jet printed transparent and flexible electrodes based on silver nanoparticles. *Journal of Materials Science: Materials in Electronics* [online]. 2018, vol. 29, no. 1, pp. 49–55 [visited on 2024-05-10]. ISSN 0957-4522, ISSN 1573-482X. Available from DOI: 10.1007/s10854-017-7886-2.

3. CHEN, Chun-Kai; LIN, Yan-Cheng; MIYANE, Satoshi; ANDO, Shinji; UEDA, Mitsuru; CHEN, Wen-Chang. Thermally and Mechanically Stable Polyimides as Flexible Substrates for Organic Field-Effect Transistors. *ACS Applied Polymer Materials* [online]. 2020, vol. 2, no. 8, pp. 3422–3432 [visited on 2024-05-10]. ISSN 2637-6105, ISSN 2637-6105. Available from DOI: 10.1021/acsapm.0c00488.

4. GAO, Zhan; YIU, Chunki; LIU, Yiming; LI, Dengfeng; MEI, Liang; ZENG, Zhiyuan; YU, Xinge. Stretchable transparent conductive elastomers for skin-integrated electronics. *Journal of Materials Chemistry C* [online]. 2020, vol. 8, no. 43, pp. 15105–15111 [visited on 2024-05-10]. ISSN 2050-7526, ISSN 2050-7534. Available from DOI: 10.1039/D0TC02913K.

5. JIA, Dongmei; XIE, Jingyi; DIRICAN, Mahmut; FANG, Dongjun; YAN, Chaoyi; LIU, Yi; LI, Chunxing; CUI, Meng; LIU, Hao; CHEN, Gang; ZHANG, Xiangwu; TAO, Jinsong. Highly smooth, robust, degradable and cost-effective modified lignin-nanocellulose green composite substrates for flexible and green electronics. *Composites Part B: Engineering* [online]. 2022, vol. 236, p. 109803 [visited on 2024-05-10]. ISSN 13598368. Available from DOI: 10.1016/j.compositesb.2022.109803.

6. XIANG, Huacui; LI, Zhijian; LIU, Hanbin; CHEN, Tao; ZHOU, Hongwei; HUANG, Wei. Green flexible electronics based on starch. *npj Flexible Electronics* [online]. 2022, vol. 6, no. 1, p. 15 [visited on 2024-02-19]. ISSN 2397-4621. Available from DOI: 10.1038/s41528-022-00147-x.

7. GUO, Zilong; WEI, Yanshang; ZHANG, Yu; XU, Yinxiao; ZHENG, Ling; ZHU, Benwei; YAO, Zhong. Carrageenan oligosaccharides: A comprehensive review of preparation, isolation, purification, structure, biological activities and applications. *Algal Research* [online]. 2022, vol. 61, p. 102593 [visited on 2024-04-29]. ISSN 22119264. Available from DOI: 10.1016/j.algal.2021.102593.

8. LAI, Danning; ZHOU, Feng; ZHOU, Arong; HAMZAH, Siti Sarah; ZHANG, Yi; HU, Jiamiao; LIN, Shaoling. Comprehensive properties of photodynamic antibacterial film based on -Carrageenan and curcumin- -cyclodextrin complex. *Carbohydrate Polymers* [online]. 2022, vol. 282, p. 119112 [visited on 2024-04-28]. ISSN 01448617. Available from DOI: 10.1016/j.carbpol.2022.119112.

9. ZHANG, Fu-Tao; XU, Lu; CHEN, Jia-Hui; ZHAO, Bo; FU, Xian-Zhu; SUN, Rong; CHEN, Qianwang; WONG, Ching-Ping. Electroless Deposition Metals on Poly(dimethylsiloxane) with Strong Adhesion As Flexible and Stretchable Conductive Materials. *ACS Applied Materials & Interfaces* [online]. 2018, vol. 10, no. 2, pp. 2075–2082 [visited on 2024-05-10]. ISSN 1944-8244, ISSN 1944-8252. Available from DOI: 10.1021/acsami.7b15726.

10. SHI, Ye; PENG, Lele; DING, Yu; ZHAO, Yu; YU, Guihua. Nanostructured conductive polymers for advanced energy storage. *Chemical Society Reviews* [online]. 2015, vol. 44, no. 19, pp. 6684–6696 [visited on 2024-05-10]. ISSN 0306-0012, ISSN 1460-4744. Available from DOI: 10.1039/C5CS00362H.

11. TIWARI, Santosh K.; KUMAR, Vijay; HUCZKO, Andrzej; ORAON, R.; ADHIKARI, A. De; NAYAK, G. C. Magical Allotropes of Carbon: Prospects and Applications. *Critical Reviews in Solid State and Materials Sciences* [online]. 2016, vol. 41, no. 4, pp. 257–317 [visited on 2024-04-29]. ISSN 1040-8436, ISSN 1547-6561. Available from DOI: 10.1080/10408436.2015.1127206.

12. YANG, Jie; HU, PingAn; YU, Gui. Design of carbon sources: starting point for chemical vapor deposition of graphene. *2D Materials* [online]. 2019, vol. 6, no. 4, p. 042003 [visited on 2024-04-29]. ISSN 2053-1583. Available from DOI: 10.1088/2053-1583/ab31bd.

13. RODRIGUEZ, R.D.; MURASTOV, G.V.; LIPOVKA, A.; FATKULLIN, M.I.; NOZDRINA, O.; PAVLOV, S.K.; POSTNIKOV, P.S.; CHEHIMI, M.M.; CHEN, Jin-Ju; SHEREMET, E. High-power laser-patterning graphene oxide: A new approach to making arbitrarily-shaped self-aligned electrodes. *Carbon* [online]. 2019, vol. 151, pp. 148–155 [visited on 2024-02-19]. ISSN 00086223. Available from DOI: 10.1016/j.carbon.2019.05.049.

14. XU, Zhen; ZHANG, Yuan; LI, Peigang; GAO, Chao. Strong, Conductive, Lightweight, Neat Graphene Aerogel Fibers with Aligned Pores. *ACS Nano* [online]. 2012, vol. 6, no. 8, pp. 7103–7113 [visited on 2024-04-30]. ISSN 1936-0851, ISSN 1936-086X. Available from DOI: 10.1021/nn3021772.

15. YAN, Jun-Xiang; LENG, Yu-Chen; GUO, Ya-Nan; WANG, Guo-Qiang; GONG, He; GUO, Pei-Zhi; TAN, Ping-Heng; LONG, Yun-Ze; LIU, Xue-Lu; HAN, Wen-Peng. Highly Conductive Graphene Paper with Vertically Aligned Reduced Graphene Oxide Sheets Fabricated by Improved Electrospray Deposition Technique. *ACS Applied Materials & Interfaces* [online]. 2019, vol. 11, no. 11, pp. 10810–10817 [visited on 2024-04-30]. ISSN 1944-8244, ISSN 1944-8252. Available from DOI: 10.1021/acsami.8b19811.

16. KASISCHKE, Maren; MARAGKAKI, Stella; VOLZ, Sergej; OSTENDORF, Andreas; GUREVICH, Evgeny L. Simultaneous nanopatterning and reduction of graphene oxide by femtosecond laser pulses. *Applied Surface Science* [online]. 2018, vol. 445, pp. 197–203 [visited on 2024-02-19]. ISSN 01694332. Available from DOI: 10.1016/j.apsusc.2018.03.086.

17. CHEN, Kunfeng; XUE, Dongfeng. Preparation of colloidal graphene in quantity by electrochemical exfoliation. *Journal of Colloid and Interface Science* [online]. 2014, vol. 436, pp. 41–46 [visited on 2024-05-10]. ISSN 00219797. Available from DOI: 10.1016/j.jcis.2014.08.057.

18. RIGHINI, Giancarlo C.; KRZAK, Justyna; LUKOWIAK, Anna; MACRELLI, Guglielmo; VARAS, Stefano; FERRARI, Maurizio. From flexible electronics to flexible photonics: A brief overview. *Optical Materials* [online]. 2021, vol. 115, p. 111011 [visited on 2024-04-28]. ISSN 09253467. Available from DOI: 10.1016/j.optmat.2021.111011.

19. KANG, Jiheong; SON, Donghee; WANG, Ging-Ji Nathan; LIU, Yuxin; LOPEZ, Jeffrey; KIM, Yeongin; OH, Jin Young; KATSUMATA, Toru; MUN, Jaewan; LEE, Yeongjun; JIN, Lihua; TOK, Jeffrey B.-H.; BAO, Zhenan. Tough and Water-Insensitive Self-Healing Elastomer for Robust Electronic Skin. *Advanced Materials* [online]. 2018, vol. 30, no. 13, p. 1706846 [visited on 2024-04-28]. ISSN 0935-9648, ISSN 1521-4095. Available from DOI: 10.1002/adma.201706846.

20. LINGHU, Changhong; ZHANG, Shun; WANG, Chengjun; SONG, Jizhou. Transfer printing techniques for flexible and stretchable inorganic electronics. *npj Flexible Electronics* [online]. 2018, vol. 2, no. 1, p. 26 [visited on 2024-04-28]. ISSN 2397-4621. Available from DOI: 10.1038/s41528-018-0037-x.

21. KAMYSHNY, Alexander; MAGDASSI, Shlomo. Conductive nanomaterials for 2D and 3D printed flexible electronics. *Chemical Society Reviews* [online]. 2019, vol. 48, no. 6, pp. 1712–1740 [visited on 2024-04-28]. ISSN 0306-0012, ISSN 1460-4744. Available from DOI: 10.1039/C8CS00738A.

22. CORZO, Daniel; TOSTADO-BLÁZQUEZ, Guillermo; BARAN, Derya. Flexible Electronics: Status, Challenges and Opportunities. *Frontiers in Electronics* [online]. 2020, vol. 1, p. 594003 [visited on 2024-04-28]. ISSN 2673-5857. Available from DOI: 10.3389/felec.2020.594003.

23. DAN, Li; SHI, Sophie; CHUNG, Hyun-Joong; ELIAS, Anastasia. Porous Polydimethylsiloxane–Silver Nanowire Devices for Wearable Pressure Sensors. *ACS Applied Nano Materials* [online]. 2019, vol. 2, no. 8, pp. 4869–4878 [visited on 2024-04-29]. ISSN 2574-0970, ISSN 2574-0970. Available from DOI: 10.1021/acsanm.9b00807.

24. AL-MILAJI, Karam Nashwan; HUANG, Qijin; LI, Zhen; NG, Tse Nga; ZHAO, Hong. Direct Embedment and Alignment of Silver Nanowires by Inkjet Printing for Stretchable Conductors. *ACS Applied Electronic Materials* [online]. 2020, vol. 2, no. 10, pp. 3289–3298 [visited on 2024-04-29]. ISSN 2637-6113, ISSN 2637-6113. Available from DOI: 10.1021/acsaelm.0c00616.

25. BOBRINETSKIY, I.I.; EMELIANOV, A.V.; SMAGULOVA, S.A.; KOMAROV, I.A.; OTERO, N.; ROMERO, P.M. Laser direct 3D patterning and reduction of graphene oxide film on polymer substrate. *Materials Letters* [online]. 2017, vol. 187, pp. 20–23 [visited on 2024-02-19]. ISSN 0167577X. Available from DOI: 10.1016/j.matlet.2016.10.073.

26. CHOI, Moon Kee; YANG, Jiwoong; HYEON, Taeghwan; KIM, Dae-Hyeong. Flexible quantum dot light-emitting diodes for next-generation displays. *npj Flexible Electronics* [online]. 2018, vol. 2, no. 1, p. 10 [visited on 2024-04-29]. ISSN 2397-4621. Available from DOI: 10.1038/s41528-018-0023-3.

27. CHEN, Shuwen; QI, Jiaming; FAN, Shicheng; QIAO, Zheng; YEO, Joo Chuan; LIM, Chwee Teck. Flexible Wearable Sensors for Cardiovascular Health Monitoring. *Advanced Healthcare Materials* [online]. 2021, vol. 10, no. 17, p. 2100116 [visited on 2024-04-29]. ISSN 2192-2640, ISSN 2192-2659. Available from DOI: 10.1002/adhm.202100116.

28. HASSAN, Muhammad; ABBAS, Ghulam; LI, Ning; AFZAL, Annum; HAIDER, Zeeshan; AHMED, Saad; XU, Xiuru; PAN, Caofeng; PENG, Zhengchun. Significance of Flexible Substrates for Wearable and Implantable Devices: Recent Advances and Perspectives. *Advanced Materials Technologies* [online]. 2022, vol. 7, no. 3, p. 2100773 [visited on 2024-05-10]. ISSN 2365-709X, ISSN 2365-709X. Available from DOI: 10.1002/admt.202100773.

29. THERKELSEN, Georg H. CARRAGEENAN. In: *Industrial Gums* [online]. Elsevier, 1993, pp. 145–180 [visited on 2024-04-29]. ISBN 9780080926544. Available from DOI: 10.1016/B978-0-08-092654-4.50011-5.

30. JIAO, Guangling; YU, Guangli; ZHANG, Junzeng; EWART, H. Chemical Structures and Bioactivities of Sulfated Polysaccharides from Marine Algae. *Marine Drugs* [online]. 2011, vol. 9, no. 2, pp. 196–223 [visited on 2024-04-29]. ISSN 1660-3397. Available from DOI: 10.3390/md9020196.

31. MONTERO, P.; PÉREZ-MATEOS, M. Effects of Na+, K+ and Ca2+ on gels formed from fish mince containing a carrageenan or alginate. *Food Hydrocolloids* [online]. 2002, vol. 16, no. 4, pp. 375–385 [visited on 2024-04-29]. ISSN 0268005X. Available from DOI: 10.1016/S0268-005X(01)00110-2.

32. FERDIANSYAH, Rival; ABDASSAH, Marline; ZAINUDDIN, Achmad; RACHMANIAR, Revika; CHAERUNISAA, Anis Yohana. Effects of Alkaline Solvent Type and pH on Solid Physical Properties of Carrageenan from Eucheuma cottonii. *Gels* [online]. 2023, vol. 9, no. 5, p. 397 [visited on 2024-04-29]. ISSN 2310-2861. Available from DOI: 10.3390/gels9050397.

33. YOUSSOUF, Latufa; LALLEMAND, Laura; GIRAUD, Pierre; SOULÉ, Faiza; BHAW-LUXIMON, Archana; MEILHAC, Olivier; D'HELLENCOURT, Christian Lefèbvre; JHURRY, Dhanjay; COUPRIE, Joël. Ultrasound-assisted extraction and structural characterization by NMR of alginates and carrageenans from seaweeds. *Carbohydrate Polymers* [online]. 2017, vol. 166, pp. 55–63 [visited on 2024-04-29]. ISSN 01448617. Available from DOI: 10.1016/j.carbpol.2017.01.041.

34. RUDKE, Adenilson Renato; DA SILVA, Mayara; ANDRADE, Cristiano José De; VITALI, Luciano; FERREIRA, Sandra Regina Salvador. Green extraction of phenolic compounds and carrageenan from the red alga Kappaphycus alvarezii. *Algal Research* [online]. 2022, vol. 67, p. 102866 [visited on 2024-04-29]. ISSN 22119264. Available from DOI: 10.1016/j.algal.2022.102866.

35. CHENG, Cheng; CHEN, Shuai; SU, Jiaqi; ZHU, Ming; ZHOU, Mingrui; CHEN, Tianming; HAN, Yahong. Recent advances in carrageenan-based films for food packaging applications. *Frontiers in Nutrition* [online]. 2022, vol. 9, p. 1004588 [visited on 2024-04-29]. ISSN 2296-861X. Available from DOI: 10.3389/fnut.2022.1004588.

36. AGA, Mohsin B.; DAR, Aamir H.; NAYIK, Gulzar A.; PANESAR, Parmjit S.; ALLAI, Farhana; KHAN, Shafat A.; SHAMS, Rafeeya; KENNEDY, John F.; ALTAF, Aayeena. Recent insights into carrageenan-based bio-nanocomposite polymers in food applications: A review. *International Journal of Biological Macromolecules* [online]. 2021, vol. 192, pp. 197–209 [visited on 2024-04-29]. ISSN 01418130. Available from DOI: 10.1016/j.ijbiomac.2021.09.212.

37. SHAFIE, Muhammad Hakimin; KAMAL, Mohd Lias; ZULKIFLEE, Fathin Farhah; HASAN, Sharizal; UYUP, Noor Hafizah; ABDULLAH, Shafinas; MOHAMED HUSSIN, Nur Ain; TAN, Yong Chia; ZAFARINA, Zainuddin. Application of Carrageenan extract from red seaweed (Rhodophyta) in cosmetic products: A review. *Journal of the Indian Chemical Society* [online]. 2022, vol. 99, no. 9, p. 100613 [visited on 2024-04-29]. ISSN 00194522. Available from DOI: 10.1016/j.jics.2022.100613.

38. CHRISTIAN, Meganne; MAZZARO, Raffaello; MORANDI, Vittorio. Bioinspired Design of Graphene-Based Materials. *Advanced Functional Materials* [online]. 2020, vol. 30, no. 51, p. 2007458 [visited on 2024-02-19]. ISSN 1616-301X, ISSN 1616-3028. Available from DOI: 10.1002/adfm.202007458.

39. NOVOSELOV, K. S.; GEIM, A. K.; MOROZOV, S. V.; JIANG, D.; ZHANG, Y.; DUBONOS, S. V.; GRIGORIEVA, I. V.; FIRSOV, A. A. Electric Field Effect in Atomically Thin Carbon Films. *Science* [online]. 2004, vol. 306, no.

5696, pp. 666–669 [visited on 2024-04-29]. ISSN 0036-8075, ISSN 1095-9203. Available from DOI: 10.1126/science.1102896.

40. WALLACE, P. R. The Band Theory of Graphite. *Physical Review* [online]. 1947, vol. 71, no. 9, pp. 622–634 [visited on 2024-04-29]. ISSN 0031-899X. Available from DOI: 10.1103/PhysRev.71.622.

41. BOEHM, H.P.; SETTON, R.; STUMPP, E. Nomenclature and terminology of graphite intercalation compounds. *Carbon* [online]. 1986, vol. 24, no. 2, pp. 241–245 [visited on 2024-04-29]. ISSN 00086223. Available from DOI: 10.1016/0008-6223(86)90126-0.

42. ASGHAR, Salva; AL-QOYYIM, Thufail Mujaddid; DIARTA, Muhamad Hendri; DOYAN, Aris. Graphene: The Revolutionary 2D Material. *Jurnal Penelitian Pendidikan IPA* [online]. 2023, vol. 9, no. 5, pp. 34–38 [visited on 2024-04-29]. ISSN 2407-795X, ISSN 2460-2582. Available from DOI: 10.29303/jppipa.v9i5.3748.

43. LI, Dan; KANER, Richard B. Graphene-Based Materials. *Science* [online]. 2008, vol. 320, no. 5880, pp. 1170–1171 [visited on 2024-04-29]. ISSN 0036-8075, ISSN 1095-9203. Available from DOI: 10.1126/science.1158180.

44. KONSCHUH, Sergej; GMITRA, Martin; FABIAN, Jaroslav. Tight-binding theory of the spin-orbit coupling in graphene. *Physical Review B* [online]. 2010, vol. 82, no. 24, p. 245412 [visited on 2024-04-29]. ISSN 1098-0121, ISSN 1550-235X. Available from DOI: 10.1103/PhysRevB.82.245412.

45. ANDREI, Eva Y; LI, Guohong; DU, Xu. Electronic properties of graphene: a perspective from scanning tunneling microscopy and magnetotransport. *Reports on Progress in Physics* [online]. 2012, vol. 75, no. 5, p. 056501 [visited on 2024-04-29]. ISSN 0034-4885, ISSN 1361-6633. Available from DOI: 10.1088/0034-4885/75/5/056501.

46. KUMAR, Manoharan Arun; JAYAVEL, Ramasamy; ARIVANANDHAN, Mukannan; RAJ, Balwinder; MOHANKUMAR, N. Performance Enhancement and Comparison of Graphene Field Effect Transistor Devices Coated with HMDS Layer. *Silicon* [online]. 2022, vol. 14, no. 16, pp. 10467–10474 [visited on 2024-04-29]. ISSN 1876-990X, ISSN 1876-9918. Available from DOI: 10.1007/s12633-022-01773-w.

47. MOROZOV, S. V.; NOVOSELOV, K. S.; KATSNELSON, M. I.; SCHEDIN, F.; ELIAS, D. C.; JASZCZAK, J. A.; GEIM, A. K. Giant Intrinsic Carrier Mobilities in Graphene and Its Bilayer. *Physical Review Letters* [online]. 2008, vol. 100, no. 1, p. 016602 [visited on 2024-04-29]. ISSN 0031-9007, ISSN 1079-7114. Available from DOI: 10.1103/PhysRevLett.100.016602.

48. NAIR, R. R.; BLAKE, P.; GRIGORENKO, A. N.; NOVOSELOV, K. S.; BOOTH, T. J.; STAUBER, T.; PERES, N. M. R.; GEIM, A. K. Fine Structure Constant Defines Visual Transparency of Graphene. *Science* [online]. 2008, vol. 320, no. 5881, pp. 1308–1308 [visited on 2024-04-29]. ISSN 0036-8075, ISSN 1095-9203. Available from DOI: 10.1126/science.1156965.

49. SUN, Yue; CAO, Yue; YI, Yunji; TIAN, Liang; ZHENG, Yao; ZHENG, Jie; WANG, Fei; ZHANG, Daming. A low-power consumption MZI thermal optical switch with a graphene-assisted heating layer and air trench. *RSC Advances* [online]. 2017, vol. 7, no. 63, pp. 39922–39927 [visited on 2024-04-29]. ISSN 2046-2069. Available from DOI: 10.1039/C7RA06463B.

50. MONTANARO, A.; WEI, W.; DE FAZIO, D.; SASSI, U.; SOAVI, G.; AVERSA, P.; FERRARI, A. C.; HAPPY, H.; LEGAGNEUX, P.; PALLECCHI, E. Optoelectronic mixing with high-frequency graphene transistors. *Nature Communications* [online]. 2021, vol. 12, no. 1, p. 2728 [visited on 2024-04-29]. ISSN 2041-1723. Available from DOI: 10.1038/s41467-021-22943-1.

51. XUE, Fei; ZHANG, Chenhui; MA, Yinchang; WEN, Yan; HE, Xin; YU, Bin; ZHANG, Xixiang. Integrated Memory Devices Based on 2D Materials. *Advanced Materials* [online]. 2022, vol. 34, no. 48, p. 2201880 [visited on 2024-04-29]. ISSN 0935-9648, ISSN 1521-4095. Available from DOI: 10.1002/adma.202201880.

52. WEI, Yuhong; LI, Xiaoshi; WANG, Yunfan; HIRTZ, Thomas; GUO, Zhanfeng; QIAO, Yancong; CUI, Tianrui; TIAN, He; YANG, Yi; REN, Tian-Ling. Graphene-Based Multifunctional Textile for Sensing and Actuating. *ACS Nano* [online]. 2021, vol. 15, no. 11, pp. 17738–17747 [visited on 2024-04-29]. ISSN 1936-0851, ISSN 1936-086X. Available from DOI: 10.1021/acsnano.1c05701.

53. KOO, Donghwan; JUNG, Sungwoo; SEO, Jihyung; JEONG, Gyujeong; CHOI, Yunseong; LEE, Junghyun; LEE, Sang Myeon; CHO, Yongjoon; JEONG, Mingyu; LEE, Jungho; OH, Jiyeon; YANG, Changduk; PARK, Hyesung. Flexible Organic Solar Cells Over 15% Efficiency with Polyimide-Integrated Graphene Electrodes. *Joule* [online]. 2020, vol. 4, no. 5, pp. 1021–1034 [visited on 2024-04-29]. ISSN 25424351. Available from DOI: 10.1016/j.joule.2020.02.012.

54. CHOI, Jae Hong; LEE, Junghyun; BYEON, Mirang; HONG, Tae Eun; PARK, Hyesung; LEE, Chang Young. Graphene-Based Gas Sensors with High Sensitivity and Minimal Sensor-to-Sensor Variation. *ACS Applied Nano Materials* [online]. 2020, vol. 3, no. 3, pp. 2257–2265 [visited on 2024-04-29]. ISSN 2574-0970, ISSN 2574-0970. Available from DOI: 10.1021/acsanm.9b02378.

55. ARKOWSKI, Jacek; OBREMSKA, Marta; KĘDZIERSKI, Kamil; SŁAWUTA, Agnieszka; WAWRZYŃSKA, Magdalena. Applications for graphene and its derivatives in medical devices: Current knowledge and future applications. *Advances in Clinical and Experimental Medicine* [online]. 2020, vol. 29, no. 12, pp. 1497–1504 [visited on 2024-04-29]. ISSN 1899-5276. Available from DOI: 10.17219/acem/130601.

56. WANG, Xiuya; WAN, Ke; XIE, Pengbo; MIAO, Yuanyuan; LIU, Zhenbo. Ultralight, High Capacitance, Mechanically Strong Graphene-Cellulose Aerogels. *Molecules* [online]. 2021, vol. 26, no. 16, p. 4891 [visited on 2024-04-29]. ISSN 1420-3049. Available from DOI: 10.3390/molecules26164891.

57. *20 let s grafenem* [online]. [N.d.]. [visited on 2024-04-29]. Available from: https://vesmir.cz/cz/casopis/archiv-casopisu/2024/cislo-2/20-let-grafenem.html.

58. VAN NOORDEN, Richard. Production: Beyond sticky tape. *Nature* [online]. 2012, vol. 483, no. 7389, S32–S33 [visited on 2024-04-29]. ISSN 0028-0836, ISSN 1476-4687. Available from DOI: 10.1038/483S32a.

59. YU, Pengxiang; WANG, Xiao; ZHANG, Kangmin; ZHOU, Dengjian; WU, Mingyuan; WU, Qingyun; LIU, Jiuyi; YANG, Jianjun; ZHANG, Jianan. Aqueous cellulose solution assisted direct exfoliation of graphite to high concentration graphene dispersion. *Materials Letters* [online]. 2021, vol. 285, p. 129081 [visited on 2024-04-29]. ISSN 0167577X. Available from DOI: 10.1016/j.matlet.2020.129081.

60. YOUNG, Katherine T.; SMITH, Colter; KRENTZ, Timothy M.; HITCHCOCK, Dale A.; VOGEL, Eric M. Graphene synthesized by chemical vapor deposition as a hydrogen isotope permeation barrier. *Carbon* [online]. 2021, vol. 176, pp. 106–117 [visited on 2024-04-29]. ISSN 00086223. Available from DOI: 10.1016/j.carbon.2021.01.127.

61. ZHANG, Weiwei; VAN DUIN, Adri C. T. Atomistic-Scale Simulations of the Graphene Growth on a Silicon Carbide Substrate Using Thermal Decomposition and Chemical Vapor Deposition. *Chemistry of Materials* [online]. 2020, vol. 32, no. 19, pp. 8306–8317 [visited on 2024-04-29]. ISSN 0897-4756, ISSN 1520-5002. Available from DOI: 10.1021/acs.chemmater.0c02121.

62. ZHENG, Qi-Fang; GUO, Yuan; LIANG, Yue; SHEN, Qing. Graphene Nanoribbons from Electrostatic-Force-Controlled Electric Unzipping of Single- and Multi-Walled Carbon Nanotubes. *ACS Applied Nano Materials* [online]. 2020, vol. 3, no. 5, pp. 4708–4716 [visited on 2024-04-29]. ISSN 2574-0970, ISSN 2574-0970. Available from DOI: 10.1021/acsanm.0c00710.

63. SENYUK, Bohdan; BEHABTU, Natnael; MARTINEZ, Angel; LEE, Taewoo; TSENTALOVICH, Dmitri E.; CERIOTTI, Gabriel; TOUR, James M.; PASQUALI, Matteo; SMALYUKH, Ivan I. Three-dimensional patterning of solid microstructures through laser reduction of colloidal graphene oxide in liquid-crystalline dispersions. *Nature Communications* [online]. 2015, vol. 6, no. 1, p. 7157 [visited on 2024-02-19]. ISSN 2041-1723. Available from DOI: 10.1038/ncomms8157.

64. GAO, Enlai; LIN, Shao-Zhen; QIN, Zhao; BUEHLER, Markus J.; FENG, Xi-Qiao; XU, Zhiping. Mechanical exfoliation of two-dimensional materials. *Journal of the Mechanics and Physics of Solids* [online]. 2018, vol. 115, pp. 248–262 [visited on 2024-04-29]. ISSN 00225096. Available from DOI: 10.1016/j.jmps.2018.03.014.

65. URADE, Akanksha R.; LAHIRI, Indranil; SURESH, K. S. Graphene Properties, Synthesis and Applications: A Review. *JOM* [online]. 2023, vol. 75, no. 3, pp. 614–630 [visited on 2024-04-29]. ISSN 1047-4838, ISSN 1543-1851. Available from DOI: 10.1007/s11837-022-05505-8.

66. ZOU, Tingting; ZHAO, Bo; XIN, Wei; WANG, Ye; WANG, Bin; ZHENG, Xin; XIE, Hongbo; ZHANG, Zhiyu; YANG, Jianjun; GUO, Chunlei. High-speed femtosecond laser plasmonic lithography and reduction of graphene oxide for anisotropic photoresponse. *Light: Science & Applications* [online]. 2020, vol. 9, no. 1, p. 69 [visited on 2024-02-19]. ISSN 2047-7538. Available from DOI: 10.1038/s41377-020-0311-2.

67. SHIN, Dong Seok; KIM, Hyun Gu; AHN, Ho Seon; JEONG, Hu Young; KIM, Youn-Jung; ODKHUU, Dorj; TSOGBADRAKH, N.; LEE, Han-Bo-Ram; KIM, Byung Hoon. Distribution of oxygen functional groups of graphene oxide obtained from low-temperature atomic layer deposition of titanium oxide. *RSC Advances* [online]. 2017, vol. 7, no. 23, pp. 13979–13984 [visited on 2024-04-30]. ISSN 2046-2069. Available from DOI: 10.1039/C7RA00114B.

68. JIŘÍČKOVÁ, Adéla; JANKOVSKÝ, Ondřej; SOFER, Zdeněk; SEDMIDUBSKÝ, David. Synthesis and Applications of Graphene Oxide. *Materials* [online]. 2022, vol. 15, no. 3, p. 920 [visited on 2024-04-30]. ISSN 1996-1944. Available from DOI: 10.3390/ma15030920.

69. LERF, Anton; HE, Heyong; FORSTER, Michael; KLINOWSKI, Jacek. Structure of Graphite Oxide Revisited. *The Journal of Physical Chemistry B* [online]. 1998, vol. 102, no. 23, pp. 4477–4482 [visited on 2024-04-30]. ISSN 1520-6106, ISSN 1520-5207. Available from DOI: 10.1021/jp9731821.

70. LONG, Donghui; LI, Wei; LING, Licheng; MIYAWAKI, Jin; MOCHIDA, Isao; YOON, Seong-Ho. Preparation of Nitrogen-Doped Graphene Sheets by a Combined Chemical and Hydrothermal Reduction of Graphene Oxide. *Langmuir* [online]. 2010, vol. 26, no. 20, pp. 16096–16102 [visited on 2024-04-30]. ISSN 0743-7463, ISSN 1520-5827. Available from DOI: 10.1021/la102425a.

71. KOTSYUBYNSKY, V.O.; BOYCHUK, V.M.; BUDZULIAK, I.M.; RACHIY, B.I.; ZAPUKHLYAK, R.I.; HODLEVSKA, M.A.; KACHMAR, A.I.; BILOGUBKA, O.R.; MALAKHOV, A.A. Structural, morphological and electrical properties of graphene oxides obtained by Hummers, Tour and modified methods: a comparative study. *Physics and Chemistry of Solid State* [online]. 2021, vol. 22, no. 1, pp. 31–38 [visited on 2024-04-29]. ISSN 2309-8589, ISSN 1729-4428. Available from DOI: 10.15330/pcss.22.1.31-38.

72. PARVEZ, Khaled; YANG, Sheng; FENG, Xinliang; MÜLLEN, Klaus. Exfoliation of graphene via wet chemical routes. *Synthetic Metals* [online]. 2015, vol. 210, pp. 123–132 [visited on 2024-04-30]. ISSN 03796779. Available from DOI: 10.1016/j.synthmet.2015.07.014.

73. HUMMERS, William S.; OFFEMAN, Richard E. Preparation of Graphitic Oxide. *Journal of the American Chemical Society* [online]. 1958, vol. 80, no. 6, pp. 1339–1339 [visited on 2024-04-30]. ISSN 0002-7863, ISSN 1520-5126. Available from DOI: 10.1021/ja01539a017.

74. GUERRERO-CONTRERAS, Jesus; CABALLERO-BRIONES, F. Graphene oxide powders with different oxidation degree, prepared by synthesis variations of the Hummers method. *Materials Chemistry and Physics* [online]. 2015, vol. 153, pp. 209–220 [visited on 2024-04-30]. ISSN 02540584. Available from DOI: 10.1016/j.matchemphys.2015.01.005.

75. MARCANO, Daniela C.; KOSYNKIN, Dmitry V.; BERLIN, Jacob M.; SINITSKII, Alexander; SUN, Zhengzong; SLESAREV, Alexander; ALEMANY, Lawrence B.; LU, Wei; TOUR, James M. Improved Synthesis of Graphene Oxide. *ACS Nano* [online]. 2010, vol. 4, no. 8, pp. 4806–4814 [visited on 2024-04-30]. ISSN 1936-0851, ISSN 1936-086X. Available from DOI: 10.1021/nn1006368.

76. BECERRA-PANIAGUA, Dulce K.; SOTELO-LERMA, M.; HU, Hailin. Highly oxidized and exfoliated graphene using a modified Tour approach. *Journal of Materials Science: Materials in Electronics* [online]. 2019, vol. 30, no. 4, pp. 3973–3983 [visited on 2024-04-30]. ISSN 0957-4522, ISSN 1573-482X. Available from DOI: 10.1007/s10854-019-00683-9.

77. KORNILOV, D. Yu.; GUBIN, S. P. Graphene Oxide: Structure, Properties, Synthesis, and Reduction (A Review). *Russian Journal of Inorganic Chemistry* [online]. 2020, vol. 65, no. 13, pp. 1965–1976 [visited on 2024-04-30]. ISSN 0036-0236, ISSN 1531-8613. Available from DOI: 10.1134/S0036023620130021.

78. TIAN, Suyun; YANG, Siwei; HUANG, Tao; SUN, Jing; WANG, Huishan; PU, Xipeng; TIAN, Linfan; HE, Peng; DING, Guqiao; XIE, Xiaoming. One-step fast electrochemical fabrication of water-dispersible graphene. *Carbon* [online]. 2017, vol. 111, pp. 617–621 [visited on 2024-04-29]. ISSN 00086223. Available from DOI: 10.1016/j.carbon.2016.10.044.

79. ZHANG, Yuan; XU, Youlong; LIU, Ruizhuo. Regulating cations and solvents of the electrolyte for ultra-efficient electrochemical production of high-quality graphene. *Carbon* [online]. 2021, vol. 176, pp. 157–167 [visited on 2024-04-29]. ISSN 00086223. Available from DOI: 10.1016/j.carbon.2021.01.109.

80. TARCAN, Raluca; TODOR-BOER, Otto; PETROVAI, Ioan; LEORDEAN, Cosmin; ASTILEAN, Simion; BOTIZ, Ioan. Reduced graphene oxide today. *Journal of Materials Chemistry C* [online]. 2020, vol. 8, no. 4, pp. 1198–1224 [visited on 2024-05-01]. ISSN 2050-7526, ISSN 2050-7534. Available from DOI: 10.1039/C9TC04916A.

81. WANG, Yi-Ming; ZHANG, Chun-Hua. Reduced Graphene Oxide Derived from Low-Grade Coal for High-Performance Flexible Supercapacitors with Ultrahigh Cyclability. *Nanomaterials* [online]. 2022, vol. 12, no. 17, p. 2989 [visited on 2024-05-01]. ISSN 2079-4991. Available from DOI: 10.3390/nano12172989.

82. PARK, Sungjin; AN, Jinho; POTTS, Jeffrey R.; VELAMAKANNI, Aruna; MURALI, Shanthi; RUOFF, Rodney S. Hydrazine-reduction of graphite- and graphene oxide. *Carbon* [online]. 2011, vol. 49, no. 9, pp. 3019–3023 [visited on 2024-05-01]. ISSN 00086223. Available from DOI: 10.1016/j.carbon.2011.02.071.

83. GUO, Juan; REN, Lulu; WANG, Ruiyu; ZHANG, Chao; YANG, Yang; LIU, Tianxi. Water dispersible graphene noncovalently functionalized with tryptophan and its poly(vinyl alcohol) nanocomposite. *Composites Part B: Engineering* [online]. 2011, vol. 42, no. 8, pp. 2130–2135 [visited on 2024-05-01]. ISSN 13598368. Available from DOI: 10.1016/j.compositesb.2011.05.008.

84. PEI, Songfeng; CHENG, Hui-Ming. The reduction of graphene oxide. *Carbon* [online]. 2012, vol. 50, no. 9, pp. 3210–3228 [visited on 2024-05-01]. ISSN 00086223. Available from DOI: 10.1016/j.carbon.2011.11.010.

85. FENG, Jianlang; YE, Yunqing; XIAO, Meng; WU, Gang; KE, Yu. Synthetic routes of the reduced graphene oxide. *Chemical Papers* [online]. 2020, vol. 74, no. 11, pp. 3767–3783 [visited on 2024-05-01]. ISSN 2585-7290, ISSN 1336-9075. Available from DOI: 10.1007/s11696-020-01196-0.

86. WANG, Gongming; QIAN, Fang; SALTIKOV, Chad W.; JIAO, Yongqin; LI, Yat. Microbial reduction of graphene oxide by Shewanella. *Nano Research* [online]. 2011, vol. 4, no. 6, pp. 563–570 [visited on 2024-05-01]. ISSN 1998-0124, ISSN 1998-0000. Available from DOI: 10.1007/s12274-011-0112-2.

87. RODRIGUEZ, Raul D.; BING, Ma; RUBAN, Alexey; PAVLOV, Sergey; AL HAMRY, Ammar; PRAKASH, Varnika; KHAN, Munis; MURASTOV, Gennadiy; MUKHERJEE, Ashutosh; KHAN, Zoheb; SHAH, Suhail; LIPOVKA, Anna; KANOUN, Olfa; MEHTA, Surinder K.; SHEREMET, Evgeniya. Reduced Graphene Oxide Nanostructures by Light: Going Beyond the Diffraction Limit. *Journal of Physics: Conference Series* [online]. 2018, vol. 1092, p. 012124 [visited on 2024-02-19]. ISSN 1742-6588, ISSN 1742-6596. Available from DOI: 10.1088/1742-6596/1092/1/012124.

88. YE, Ruquan; JAMES, Dustin K.; TOUR, James M. Laser-Induced Graphene. *Accounts of Chemical Research* [online]. 2018, vol. 51, no. 7, pp. 1609–1620 [visited on 2024-05-01]. ISSN 0001-4842, ISSN 1520-4898. Available from DOI: 10.1021/acs.accounts.8b00084.

89. LI, Qiang; DING, Ye; YANG, Lijun; LI, Linlin; WANG, Yang. Periodic nanopatterning and reduction of graphene oxide by femtosecond laser to construct high-performance micro-supercapacitors. *Carbon* [online]. 2021, vol. 172, pp. 144–153 [visited on 2024-02-19]. ISSN 00086223. Available from DOI: 10.1016/j.carbon.2020.09.096.

90. KYMAKIS, Emmanuel; SAVVA, Kyriaki; STYLIANAKIS, Minas M.; FOTAKIS, Costas; STRATAKIS, Emmanuel. Flexible Organic Photovoltaic Cells with In Situ Nonthermal Photoreduction of Spin-Coated Graphene Oxide Electrodes. *Advanced Functional Materials* [online]. 2013, vol. 23, no. 21,

pp. 2742–2749 [visited on 2024-05-01]. ISSN 1616-301X, ISSN 1616-3028. Available from DOI: 10.1002/adfm.201202713.

91. LIU, Zhi-Bo; ZHAO, Xin; ZHANG, Xiao-Liang; YAN, Xiao-Qing; WU, Ying-Peng; CHEN, Yong-Sheng; TIAN, Jian-Guo. Ultrafast Dynamics and Nonlinear Optical Responses from sp ^{2} - and sp ^{3} -Hybridized Domains in Graphene Oxide. *The Journal of Physical Chemistry Letters* [online]. 2011, vol. 2, no. 16, pp. 1972–1977 [visited on 2024-05-01]. ISSN 1948-7185, ISSN 1948-7185. Available from DOI: 10.1021/jz2008374.

92. HUANG, Min; ZHAO, Fuli; CHENG, Ya; XU, Ningsheng; XU, Zhizhan. Origin of Laser-Induced Near-Subwavelength Ripples: Interference between Surface Plasmons and Incident Laser. *ACS Nano* [online]. 2009, vol. 3, no. 12, pp. 4062–4070 [visited on 2024-05-01]. ISSN 1936-0851, ISSN 1936-086X. Available from DOI: 10.1021/nn900654v.

93. TRUSOVAS, Romualdas; RAČIUKAITIS, Gediminas; NIAURA, Gediminas; BARKAUSKAS, Jurgis; VALUŠIS, Gintaras; PAULIUKAITE, Rasa. Recent Advances in Laser Utilization in the Chemical Modification of Graphene Oxide and Its Applications. *Advanced Optical Materials* [online]. 2016, vol. 4, no. 1, pp. 37–65 [visited on 2024-05-01]. ISSN 2195-1071, ISSN 2195-1071. Available from DOI: 10.1002/adom.201500469.

94. LIN, Yue; JIN, Jie; KUSMARTSEVAB, Olga; SONG, Mo. Preparation of Pristine Graphene Sheets and Large-Area/Ultrathin Graphene Films for High Conducting and Transparent Applications. *The Journal of Physical Chemistry C* [online]. 2013, vol. 117, no. 33, pp. 17237–17244 [visited on 2024-05-01]. ISSN 1932-7447, ISSN 1932-7455. Available from DOI: 10.1021/jp403903k.

95. WATANABE, Akira; AMINUZZAMAN, Mohammod; CAI, Jinguang; AKHTARUZZAMAN, Md.; OGAWA, Sayaka; AOYAGI, Eiji; ITO, Shun. Laser Direct Writing of Microstructure on Graphene Oxide/Metal Oxide Hybrid Film. *Journal of Photopolymer Science and Technology* [online]. 2019, vol. 32, no. 2, pp. 223–226 [visited on 2024-05-01]. ISSN 0914-9244, ISSN 1349-6336. Available from DOI: 10.2494/photopolymer.32.223.

96. SAVILLE, Alec I.; CREUZIGER, Adam; MITCHELL, Emily B.; VOGEL, Sven C.; BENZING, Jake T.; KLEMM-TOOLE, Jonah; CLARKE, Kester D.; CLARKE, Amy J. MAUD Rietveld Refinement Software for Neutron Diffraction Texture Studies of Single- and Dual-Phase Materials. *Integrating Materials and Manufacturing Innovation* [online]. 2021, vol. 10, no. 3, pp. 461–487 [visited on 2024-05-12]. ISSN 2193-9764, ISSN 2193-9772. Available from DOI: 10.1007/s40192-021-00224-5.

97. KHASHAN, Khawla S.; JABIR, Majid S.; ABDULAMEER, Farah A. CARBON NANOPARTICLES PREPARED BY LASER ABLATION IN LIQUID ENVIRONMENT. *Surface Review and Letters* [online]. 2019, vol. 26, no. 10, p. 1950078 [visited on 2024-05-10]. ISSN 0218-625X, ISSN 1793-6667. Available from DOI: 10.1142/S0218625X19500781.

98. SCARDACI, Vittorio; COMPAGNINI, Giuseppe. Raman Spectroscopy Investigation of Graphene Oxide Reduction by Laser Scribing. *C* [online]. 2021, vol. 7, no. 2, p. 48 [visited on 2024-05-03]. ISSN 2311-5629. Available from DOI: 10.3390/c7020048.

99. JOHRA, Fatima Tuz; LEE, Jee-Wook; JUNG, Woo-Gwang. Facile and safe graphene preparation on solution based platform. *Journal of Industrial and Engineering Chemistry* [online]. 2014, vol. 20, no. 5, pp. 2883–2887 [visited on 2024-05-10]. ISSN 1226086X. Available from DOI: 10.1016/j.jiec.2013.11.022.

100. SILVA FILHO, J. C.; VENANCIO, E. C.; SILVA, S. C.; TAKIISHI, H.; MARTINEZ, L. G.; ANTUNES, R. A. A thermal method for obtention of 2 to 3 reduced graphene oxide layers from graphene oxide. *SN Applied Sciences* [online]. 2020, vol. 2, no. 8, p. 1450 [visited on 2024-05-12]. ISSN 2523-3963, ISSN 2523-3971. Available from DOI: 10.1007/s42452-020-03241-9.

101. PERUMAL, P.; SELVIN, P. Christopher. Red algae-derived k-carrageenan-based proton-conducting electrolytes for the wearable electrical devices. *Journal of Solid State Electrochemistry* [online]. 2020, vol. 24, no. 10, pp. 2249–2260 [visited on 2024-05-10]. ISSN 1432-8488, ISSN 1433-0768. Available from DOI: 10.1007/s10008-020-04724-w.

102. SANGEETHA, P.; SELVAKUMARI, T. M.; SELVASEKARAPANDIAN, S.; SRIKUMAR, S. R.; MANJULADEVI, R.; MAHALAKSHMI, M. Preparation and characterization of biopolymer K-carrageenan with MgCl2 and its application to electrochemical devices. *Ionics* [online]. 2020, vol. 26, no. 1, pp. 233–244 [visited on 2024-05-10]. ISSN 0947-7047, ISSN 1862-0760. Available from DOI: 10.1007/s11581-019-03193-0.